Chapter 5: Chemical modification of $(Me_2NH_2)[In(ABDC)_2]$ and its effect on framework flexibility

5.1 Abstract

Post-synthetic modification reactions have been carried out on the MOF $(Me_2NH_2)[In(ABDC)_2]$, involving reactions at the amino group of the 2-aminobenzenedicarboxylate (ABDC) ligand or cation exchange reactions involving partial replacement of the dimethyl ammonium cations within the MOF pores. Investigations into the effect that these modifications have on the continuous breathing effect show that both the dimensionality of the flexibility and the solvent dependence change substantially. The characterisation is mainly through crystallographic methods, including *in situ* crystallographic experiments under CO_2 pressures, which explore the effect of the modifications on the gas uptake properties.

5.2 Introduction

The interior functionalization of metal-organic frameworks (MOFs) is of particular importance in tuning their gas uptake and separation properties. Introduction of pendant amine groups for example, either by using amino-functionalized organic linkers,[1] or grafting of bifurcated amines onto open metal sites,[2, 3] has shown improvements to the gravimetric CO_2 uptakes in several rigid MOFs. Further evidence of the improvements is seen through the direct interactions of amine groups with CO_2 molecules which have been observed during *in situ* crystallographic studies on $Zn_2(Atz)_2(Ox)$ (Atz = 3-amino-1,2,4-triazole, Ox = oxalate).[4, 5] Similar favourable interactions have been seen crystallographically from triazole nitrogens in MAF-X7 and MAF-23 and hydroxyl groups in NOTT-300.[6–8] Functional groups in particular have proven highly relevant in flexible MOFs systems; the addition of polar groups, such as NH_2 and COOH, cause MIL-53(Fe) to remain locked in its closed pore structure during CO_2 uptake, whereas frameworks modified with less polar groups still show the typical multi-step phase transitions, with the required pressures for the transitions changing based on the substituent.[9] Similar control of the gating behaviour has also been demonstrated for various ether modified DMOF species, along with large variations in the extent of the breathing mode.[10]

Direct incorporation of modified ligands into metal-organic frameworks is not always possible via the normal self-assembly reaction used for MOF synthesis, but a wide variety of post-synthetic modification (PSM) methods have been developed to add / change functionalities once the framework structure has already been synthesised.[11] The modification reactions can target either

the organic linker, the counter ions present[12] or the metal ions[13], resulting in full or partial conversions. Pioneering work by Wang and Cohen on amino-functionalized paddlewheel framework DMOF has shown that the modification to an alkyl amide can stabilise the large or narrow pore form of DMOF depending on the alkyl chain length, and even turn on/off the materials breathing.[14]

$(Me_2NH_2)[In(ABDC)_2]$ is ideally suited for similar modification studies because it is a flexible MOF which incorporates both an amino group and a charge-balancing cation, offering a wide range of possible reactions. The rare breathing effect of the MOF is thought to occur due to solvent-framework or solvent-cation interactions, and by changing the functional groups, the flexibility might be able to be tuned and understood. The location of the amino group is not highly disordered unlike the situation in many MOFs that use the ABDC ligand. $(Me_2NH_2)[In(ABDC)_2]$ has one primary site therefore giving the potential for detailed structural characterisation of the outcome of post-synthetic modification. To the author's knowledge no modification studies on $(Me_2NH_2)[In(ABDC)_2]$ have previously been reported.

This chapter mainly focuses the modification with acetic anhydride to convert the amine group into a methyl amide, and the exchange of the cation for a Ag^+ ion, but preliminary results on the modification with maleic anhydride will also be covered. The conversion to the methyl amide was chosen because it is well documented in the literature, being reported for IRMOF-3,[15, 16] DMOF-NH_2,[14] MIL(Al)-53-NH_2,[17] UiO-66-NH_2,[15, 18, 19] and CAU-1-NH_2,[20] often in high conversions. In addition the reaction causes a relatively small change to the overall ligand. Ag^+ ions were used for cation exchange because they allowed easier crystallographic characterisation; the large number of electrons being obvious within the diffraction pattern even at partial occupancies. Ag^+ ions have also recently been incorporated into several MOFs, showing improvements in olefin / paraffin separations, C_2 hydrocarbon / CH_4 separations and desulfurization of fuels.[12, 21, 22]

5.3 Experimental

5.3.1 General

All reagents were purchased from Sigma-Aldrich or Alfa Aesar and were used without further purification, unless otherwise stated.

5.3.2 Synthesis

Synthesis of $(Me_2NH_2)[In(BDC\text{-}NHC(O)CH_3)_{1.5}(ABDC)_{0.5}].CHCl_3$ (**75%AM**)(Modification Method A):

Crystals from $(Me_2NH_2)[In(ABDC)_2].DMF$ (0.010 g, 0.02 mmol) were placed into 0.6 mL of HPLC grade $CHCl_3$ within a 1.5 mL screw-capped glass vial. 5 equivalents of acetic anhydride (10 µL, 0.1 mmol) were added and the vial was placed inside a temperature controlled oven. The temperature was ramped to 55 °C at 2.5 °C/min and maintained for 24 hrs before cooling to room temperature at a rate of 0.1 °C/min. Upon removal from the oven the brown diamond-shaped crystals were still present and were transferred and stored in fresh $CHCl_3$.

Synthesis of $(Me_2NH_2)[In(BDC\text{-}NHC(O)CH_3)_2].CHCl_3$ (**100%AM**)(Modification Method B):

Crystals from $(Me_2NH_2)[In(ABDC)_2].DMF$ (0.100g, 0.2 mmol) were placed into 0.6ml of HPLC grade $CHCl_3$ within a 1.5ml screw toped glass vial. 5 equivalents of acetic anhydride (100µl, 1 mmol) were added and the vial was placed inside a temperature controlled oven. The temperature was ramped to 55 °C at 2.5 °C/min and maintained for 24hrs before cooling to room temperature at a rate of 0.1 °C/min. Upon removal from the oven the brown diamond shaped crystals were still present and were transferred and stored in fresh $CHCl_3$.

Synthesis of $(Me_2NH_2)[In(BDC\text{-}NHC(O)CH_3)_2].DMF$ (**100%AM.DMF**):

Single crystals of $(Me_2NH_2)[In(BDC\text{-}NHC(O)CH_3)_2].CHCl_3$ (≈0.100 g, 0.17 mmol) were placed in DMF (1 ml), dried according to the method of Grubbs,[23] for 1-2 weeks. DMF was replaced daily.

Synthesis of $(Me_2NH_2)[In(ABDC)_{1.5}(BDC\text{-}NHC(O)CHCHC(O)OH)_{0.5}].CHCl_3$ (**25%MAL**):

Crystals from $(Me_2NH_2)[In(ABDC)_2].DMF$ (0.017g, 0.03 mmol) were placed into 0.6ml of HPLC grade $CHCl_3$ within a 1.5ml screw toped glass vial. Maleic anhydride (8.7mg, 0.09 mmol) were added and the vial was placed inside a temperature controlled oven. The temperature was ramped to 55 °C at 2.5°C/min and maintained for 24hrs before cooling to room temperature at a rate of 0.1 °C/min.

Upon removal from the oven the brown diamond shaped crystals were still present and were transferred and stored in fresh $CHCl_3$.

Synthesis of $(Me_2NH_2)_{(1-x)}Ag_x[In(ABDC)_2].DMF$ $(0.5 \leq x \leq 0.8)$ (**AgM**):

Method A: Crystals of $[In(ABDC)_2Me_2NH_2].DMF$ (0.015 g, 0.03 mmol) were soaked in 1 mL of HPLC grade DMF containing $AgNO_3$ (0.058 g, 0.34 mmol) for 1 week. The $AgNO_3$ was exchanged daily and carried out in the dark. After the reaction was finished the solvent was exchanged for fresh DMF.

Method B: Crystals of $[In(ABDC)_2Me_2NH_2].DMF$ (0.015 g, 0.03 mmol) were soaked in 1 mL of DMF containing $AgBF_4$ (0.062 g, 0.32 mmol) for 1 week. The $AgBF_4$ was exchanged daily and carried out in the dark. After the reaction was finished the solvent was exchanged for fresh DMF.

Method C: $AgNO_3$ (0.348 g, 2.05 mmol) was dissolved in 3.6 mL of DMF inside a 24 mL -capped glass vial. To this solution crystals of $[In(ABDC)_2Me_2NH_2].DMF$ (0.09 g, 0.17 mmol) were added and the vial was placed inside a temperature-controlled oven. The temperature was ramped to 55 ^oC at 2.5 ^oC/min and maintained for 24 hrs before cooling to room temperature at a rate of 0.1 ^oC/min. Upon removal from the oven the brown diamond-shaped crystals were still present and were transferred and stored in fresh DMF.

5.3.3 Analysis

TGA analyses were obtained using a Perkin Elmer Thermogravimetric Analyser under a nitrogen atmosphere. The sample (3.3 mg) was held at 25 ^oC for 30 minutes prior to heating from 25^oC to 600 ^oC at a rate of 4 ^oC/min. The exported data were plotted using Microsoft Excel.

Solution-phase ^1H NMR spectroscopy (400Mhz, DMSO-d6) was carried out using a Bruker DPX-400 spectrometer. The MOF sample (10 mg) was digested using 50 µL of acid (35% DCl in D_2O) in 1 mL of DMSO-d6, and recorded without neutralising the solution. All the constituent parts were observed to be soluble in the DMSO after the digestion.

Solid-State IR was recorded using a PerkinElmer Spectrum 100 spectrometer fitted with a universal diamond ATR accessory.

Laboratory single-crystal X-ray diffraction data were collected on a Bruker SMART APEX-II CCD diffractometer operating a Mo-K_α sealed-tube X-ray source or a Bruker D8 Venture diffractometer equipped with a PHOTON 100 dual-CMOS chip detector and operating a Cu-K_α IµS microfocus X-ray source. The data were processed using the APEX2 software.[24] X-Ray data were corrected for

absorption using empirical methods (SADABS) based upon symmetry-equivalent reflections combined with measurements at different azimuthal angles.[25, 26] Synchrotron diffraction data were recorded at beamline I19[27] at Diamond Light Source. A full hemisphere of data was collected using three 132 °, and one 180 ° omega scans at 0.4 ° slicing on a Newport diffractometer equipped with a Pilatus 300K detector. Data were recorded at a wavelength of 0.6889(1) Å, took 15 min to collect and were processed and corrected for adsorption using Agilent Crysalis Pro software.[28] An Oxford Cryosystems Cryostream device was to maintain the sample temperature in both laboratory and synchrotron set-ups. *In situ* single crystal diffraction studies of gas adsorption were carried out at beamline I19[27] Diamond Light Source, using the same parameters described above. The samples were glued to a MiTeGen 100µm Microloop using araldite adhesive and fixed inside the I19 gas cell constructed from a 1 mm quartz capillary. All crystal structures were solved and refined against F^2 values using the SHELX 2013 suite accessed within the OLEX2 program.[29, 30] Non-disordered, non-hydrogen framework atoms were refined anisotropically, but disordered framework atoms and cations were modelled with isotropic displacement parameters, using a combination of crystallographic restraints and constraints. Hydrogen atoms were placed in calculated positions with idealised geometries and then refined using a riding model with isotropic displacement parameters. Final CIFs were checked using checkCIF/PLATON.[31] The routine SQUEEZE in the program PLATON was used to obtain a residual electron count within the pore.[32] All electron counts were obtained after fully removing any modelled counter ions from the crystallographic model and re-refining the structure. The electron count related to solvent was then determined by manually subtracting to number of electron associated with the counter ions from the total contained within the unit cell.

Laboratory powder diffraction data were obtained using a Bruker D8 Advance powder diffractometer equipped with focusing Göbel mirrors, recorded in the range $4\ ^{o} \leq 2\theta \leq 50\ ^{o}$, using Cu-$K_{\alpha}$ radiation. Data were collected in a Debye-Scherrer geometry with rotating capillary stage and samples loaded in either 0.5 mm or 0.7 mm borosilicate capillaries. Sample temperature for *in situ* heating studies was controlled by a co-axial stream of dry nitrogen gas from and Oxford Cryosystems Cryostream Plus device, with a flow rate of 5 L/min. Synchrotron powder diffraction data were collected at beamline I11 at Diamond Light Source using a wide-angle (90 °) position sensitive detector (PSD) comprising 18 Mythen-2 modules.[33, 34] A pair of scans related by a 0.25 ° detector offset was collected for each measurement to account for gaps between detector modules. *In situ* powder diffraction studies of gas adsorption were carried out at beamline I11[33, 34] Diamond Light Source, using synchrotron radiation. Powdered samples were loaded into 0.5 mm or 0.7 mm quartz capillaries and glued into the I11 gas cell using araldite adhesive. The resulting patterns were summed to give the final pattern for analysis. Indexing, Pawley and Rietveld refinements were

carried out using TOPAS version 4.1[35–40] Measures of agreement between the calculated and experimental diffraction data (R_{wp} and R_{wp}') are defined by the equations below.

$$R_{wp} = \sqrt{\frac{\Sigma[w(Y_{\text{obs}} - Y_{\text{calc}})^2]}{\Sigma[wY_{\text{obs}}{}^2]}} \qquad R_{wp}{}' = \sqrt{\frac{\Sigma[w(Y_{\text{obs}} - Y_{\text{calc}})^2]}{\Sigma[w(Y_{\text{obs}} - bkgr)^2]}}$$

5.3.4 Crystallographic characterisation after post-synthetic modification reactions of $(Me_2NH_2)[In(ABDC)_2]$

Post-synthetic modification reactions were carried out on $(Me_2NH_2)[In(ABDC)_2]$ using the synthetic methods described in section 5.3.2. The reactions involved modification of the amine functionality with acetic anhydride or maleic anhydride. A schematic for the modifications is shown in Figure 1.

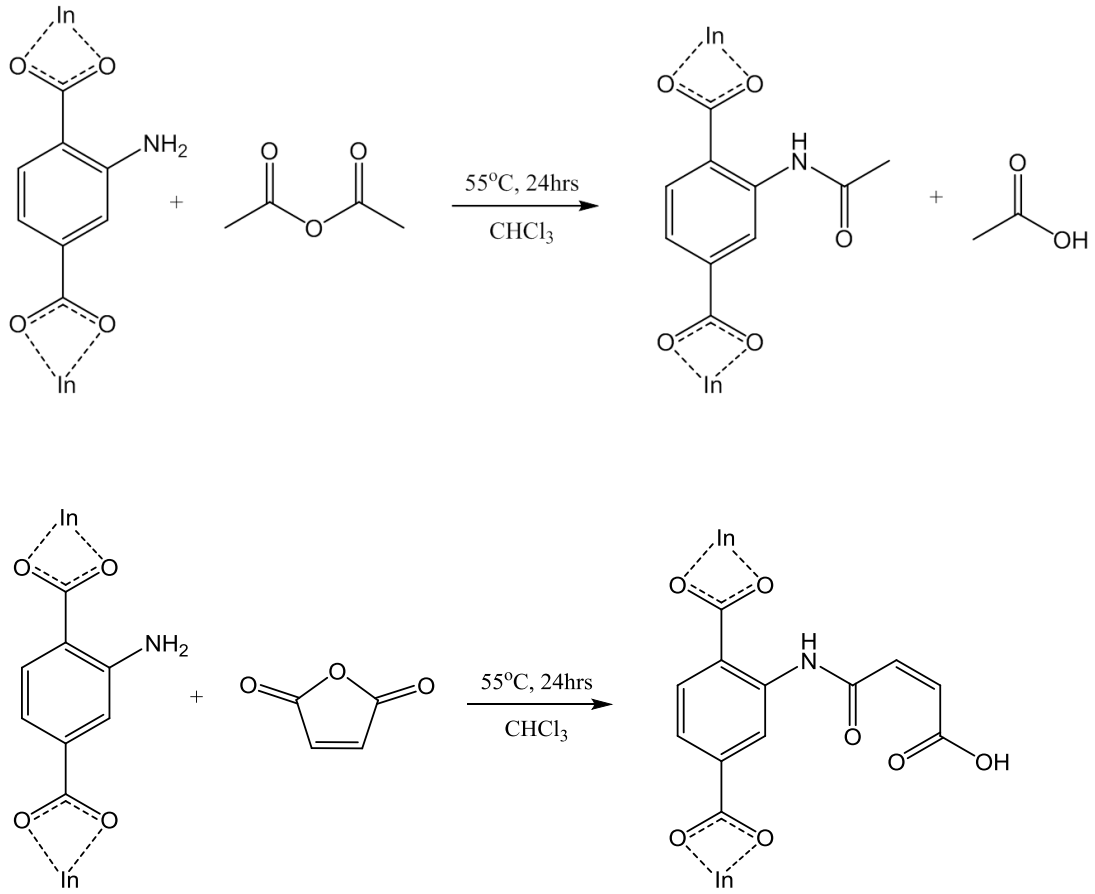

Figure 1 - Post-synthetic modification reactions carried out on amine functionality of $(Me_2NH_2)[In(ABDC)_2]$

Single crystal diffraction characterisation

Single crystals obtained after PSM reactions were directly transferred into a perfluoropolyether oil (FOMBLIN Y). The crystals were mounted onto a MiTeGen 200µm MicroMount under an optical microscope, and transferred to the diffractometer where the crystal was immersed in the dry nitrogen stream of the Cryostream device at 100K. Table 1 lists the crystal structures obtained and the relative modification percentage modelled. Full refinement parameters can be seen in Table 2. **M1** and **M2** used different synthetic methods as described in section 5.3.2.

Table 1 - Modification details and fixed chemical occupancies used in single crystal X-ray structure determinations of PSM reaction products of $(Me_2NH_2)[In(ABDC)_2]$

Crystal Code	Modification Details / Name	Modification %
M1	Acetic anhydride modification in $CHCl_3$ (Method A) Name: 75% amide-modified MOF (**75%AM**)	75
M2	Acetic anhydride modification in $CHCl_3$ (Method B) Name: 100% amide-modified MOF (**100%AM**)	100
M3	Acetic Anhydride Modification and solvent exchanged for DMF Name: 100% amide-modified MOF in DMF (**100%AM.DMF**)	100
M4	Maleic anhydride Modification in $CHCl_3$ Name: 25% Maleic anhydride modified MOF (**25%Mal**)	25

Table 2 - Data collection, structure solution and refinement parameters for single crystal X-ray structure determinations of post-synthetically modified MOFs

	75% amide modified MOF **(M1)**	100% amide modified MOF in $CHCl_3$ **(M2)**	100% amide modified MOF in DMF **(M3)**	25% Maleic anhydride modified MOF **(M4)**
Crystal Habit	Octahedron	Octahedron	Octahedron	Octahedron
Crystal Colour	Brown	Brown	Brown	Brown
Crystal Size (mm)	0.14 × 0.13 × 0.1	0.19 × 0.17 × 0.11	0.29 × 0.2 × 0.13	0.19 × 0.17 × 0.15
Crystal System	Orthorhombic	Orthorhombic	Orthorhombic	Orthorhombic
Space Group, Z	*Fddd*, 16	*Fddd*, 16	*Fddd*, 16	*Fddd*, 16
a (Å)	14.6266(7)	14.633(3)	14.7819(4)	14.683(4)
b (Å)	26.8907(12)	28.004(6)	25.4635(7)	26.783(7)
c (Å)	31.5398(15)	30.640(7)	32.6683(9)	31.433(8)
α (°)	90	90	90	90
β (°)	90	90	90	90
γ (°)	90	90	90	90
V (Å^3)	12405.2(10)	12556(5)	12296.3(6)	12361(6)
Radiation	Mo-K_α (λ = 0.71073 Å)	Cu-K_α (λ = 1.54178 Å)	Mo-K_α (λ = 0.71073 Å)	Mo-K_α (λ = 0.71073 Å)
Density (g cm^{-3})	1.247[b]	1.448[c]	1.383[c]	1.205[b]
Temperature (K)	100	100	100	100
μ (mm^{-1})[d]	0.806	7.685	0.822	0.801
2θ Range (°)	3.42 to 54.96	7.40 to 133.48	4.98 to 55.08	6.60 to 55.08
Reflns collected	29284	17599	14440	9909
Independent reflns (R_{int})	3554 (0.0602)	2780 (0.0293)	3306 (0.0536)	3298 (0.0759)
Reflns used in refinement, *n*	3554	2780	3306	3298
L.S. parameters, *p*	163	173	147	151
No. of restraints, *r*	11	7	42	13
Completeness	0.998	0.996	0.930	0.925
$R1(F)$[a] $I > 2\sigma(I)$	0.0654	0.0588	0.1216	0.0823
$wR2(F^2)$[a], all data	0.2444	0.1945	0.4493	0.3314
$S(F^2)$[a], all data	1.194	1.132	1.814	1.108

[a] $R1(F) = \sum(|F_o| - |F_c|)/\sum|F_o|$; $wR2(F^2) = \sqrt{\sum w\left(F_o^2 - F_c^2\right)^2/\sum wF_o^4}$; $S(F^2) = \sqrt{\sum w\left(F_o^2 - F_c^2\right)^2/(n+r-p)}$.

[b] Densities calculated using only framework atoms and cations, and do not include guest molecules.

[c] Densities calculated using framework atoms, cations, and modelled guest molecules.

[d] Adsorption coefficients are calculated based on the crystallographic model

SQUEEZE analysis

The electron count in the pore was calculated using the routine SQUEEZE[32] in the program PLATON.[31] following the procedure detailed in section 5.3.3. The number of electrons per cell corresponds to both solvent and cations, with the number of electrons due to solvent being determined by subtracting the number of electrons associated with the cation and dividing by the number of formula units within one unit cell.

Table 3 – Electron count and accessible void during SQUEEZE analysis of modified MOF **M1-4**

	Electrons per unit cell (in void spaces)	Solvent accessible void per unit cell (Å^3)	Electrons per Indium due to solvent [a]
M1	1360	4522.6	58
M2	1641	4882.5	76
M3	435	4295.5	0
M4	223	4123.3	-13

[a] Calculated by dividing the electron count per cell by Z and subtracting the electrons associated with the cations

Powder Diffraction characterisation

Powdered samples were prepared by filtering single crystals of the modified frameworks under vacuum, and grinding in a pestle and mortar. X-Ray diffraction data were recorded using synchrotron radiation at the I11 beamline[33] Diamond Light Source, λ = 0.82663(5) Å. Diffraction patterns were obtained for the 100% amide modified MOF **PM1**, the 100% amide modified MOF in DMF **PM2**, and 25% maleic anhydride modified MOF (**PM3**). The powder diffraction patterns are displayed in Figure 2 compared to the as-synthesised parent MOF (**P1**). All data was recorded at room temperature.

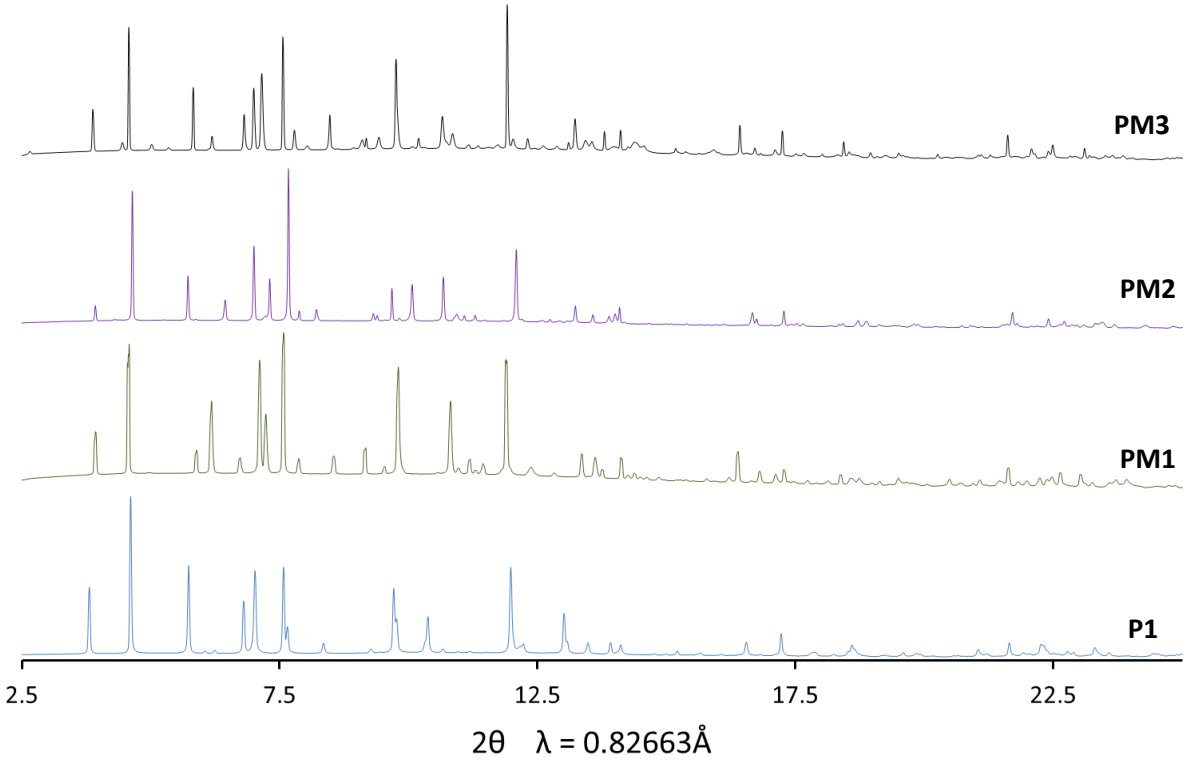

Figure 2 - X-ray powder diffraction patterns of modified frameworks **PM1-3** in comparison to parent as-synthesised MOF **P1**. Patterns have been scaled in 2θ and represented using 2θ values corresponding to λ = 0.82663 Å.

Pawley fitting of **PM1**

The phase purity of **PM1** was confirmed using a single phase Pawley[37] refinement. The unit cell parameters for the fit were initially determined using an auto indexing algorithm. The refinement employed 1,870 parameters (12 background, 1 zero error, 5 profile, 3 cell and 1,849 reflections), resulting in final indices of fit R_{wp} = 4.189, $R_{wp'}$ = 14.445. The final unit cell parameters were orthorhombic a = 14.7914 (4) Å, b = 28.132 (1) Å, c = 30.557 (1) Å, V = 12715.2 (7) Å^3. The fit is displayed in Figure 3. Several of the peaks within **PM1** were observed to be badly fit due to a slight splitting in the peak shape. Many of these peaks, however, only correspond to one set of Miller

indices in the Pawley fit. This is thought to occur due to a combination of closely related phases which were not modelled in the fitting and will be covered in detail in section 5.4.1.

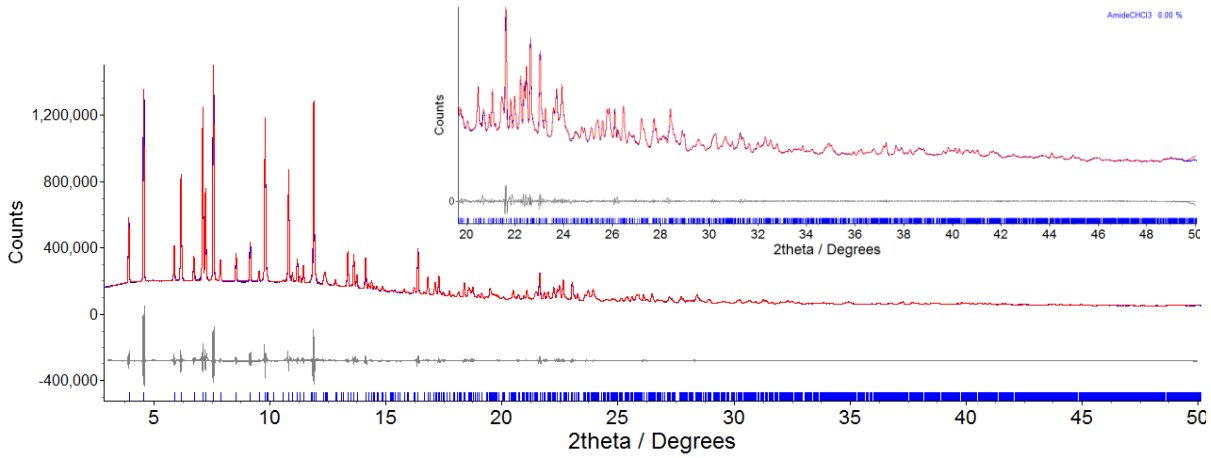

Figure 3 – Observed (blue) and calculated (red) and difference plot [I_{obs} - I_{calc}] (grey) of the Pawley[37] refinement of 75% amide-modified MOF $(Me_2NH_2)[In(BDC\text{-}NHC(O)CH_3)_2]$ (**PM1**) (2θ range 3.0 – 50.0 °, d_{min} = 0.98Å).

Pawley and Rietveld fitting of **PM2**

The identity of the structure of sample **PM2** was confirmed through both Pawley and Rietveld refinements. The unit cell parameters for the fit were initially determined using an auto indexing algorithm. The Pawley[37] refinement employed 1,855 parameters (10 background, 1 zero error, 5 profile, 3 cell and 1,836 reflections), resulting in final indices of fit R_{wp} = 3.412, $R_{wp'}$ = 10.855. The framework atoms of **M3** were then used as a starting point for a Rietveld[40] refinement employing 21 parameters (10 background, 1 zero error, 5 profile, 3 cell, 1 scale and 1 occupancy), resulting in final indices of fit R_{wp} = 5.431, $R_{wp'}$ = 18.714. The positions and orientations of the cation and solvent molecules (modelled as rigid bodies) were optimised by simulated annealing. The final unit cell parameters were orthorhombic a = 14.8774 (2) Å, b = 26.2123 (4) Å, c = 32.1573 (6) Å, V = 12540.4 (3) Å^3. The fits for the two refinements are displayed in Figure 4 and Figure 5. No splitting of the peaks was observed in sample **PM2**, resulting in a better fit to the experimental data than in **PM1**.

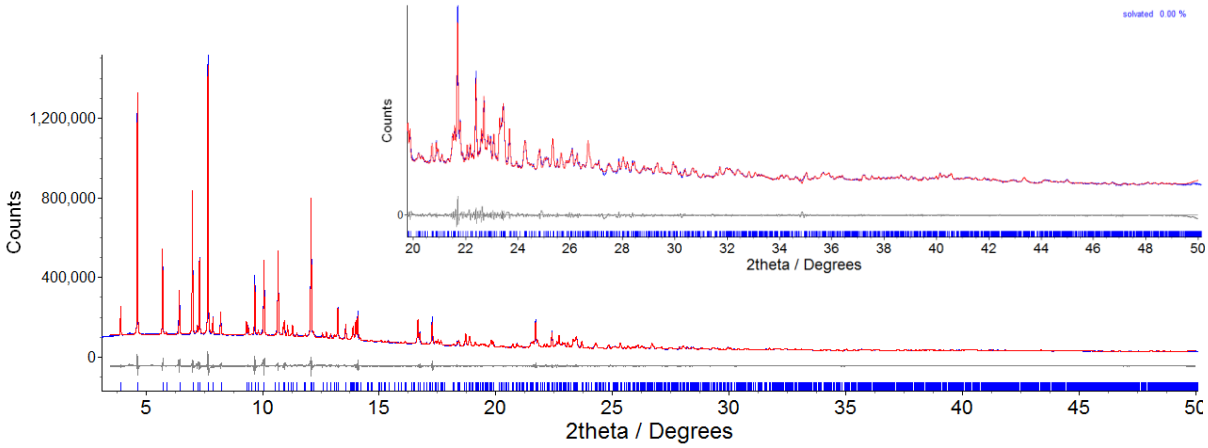

Figure 4 – Observed (blue) and calculated (red) and difference plot [I_{obs} - I_{calc}] (grey) of the Pawley[37] refinement of 100% amide-modified MOF in DMF $(Me_2NH_2)[In(BDC\text{-}NHC(O)CH_3)_2]$ (**PM2**) (2θ range 3.0 – 50.0 °, d_{min} = 0.98Å).

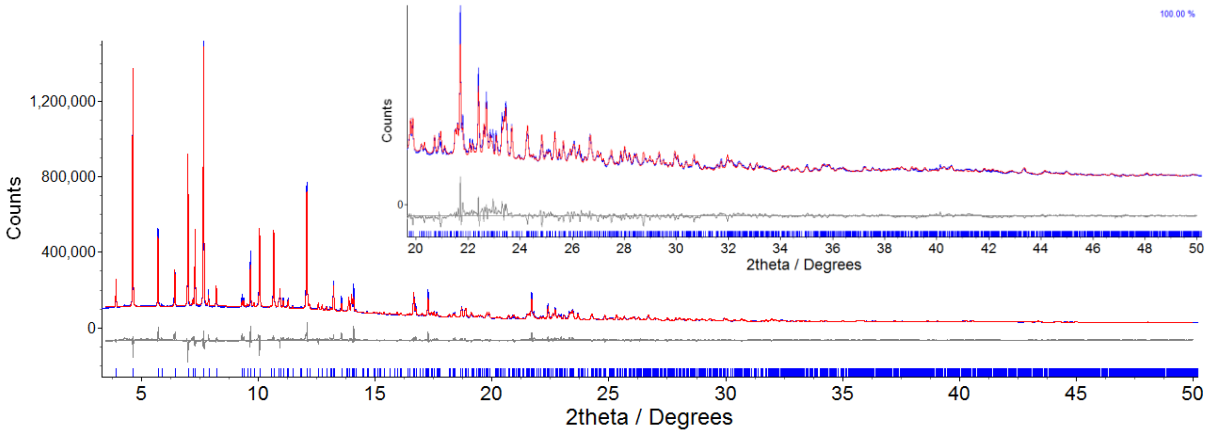

Figure 5 - Observed (blue) and calculated (red) and difference plot [I_{obs} - I_{calc}] (grey) of the Rietveld[40] refinement of 100% amide-modified MOF in DMF $(Me_2NH_2)[In(BDC\text{-}NHC(O)CH_3)_2].0.47DMF$ (**PM2**) (2θ range 3.0 – 50.0 °, d_{min} = 0.98Å).

5.3.5 Complementary characterisation techniques after post-synthetic modification reactions of $(Me_2NH_2)[In(ABDC)_2]$

NMR spectroscopy of 75% amide-modified MOF

A solution-phase ^1H NMR spectrum of the framework after the post-synthetic modification method A (**75%AM**) was obtained following the digestion procedure described in Section 5.3.3 (Figure 6). Integration of the proton environments suggests an 80% conversion of the organic ligand. A expanded section between 7.5 – 9.2ppm is shown in Figure 7

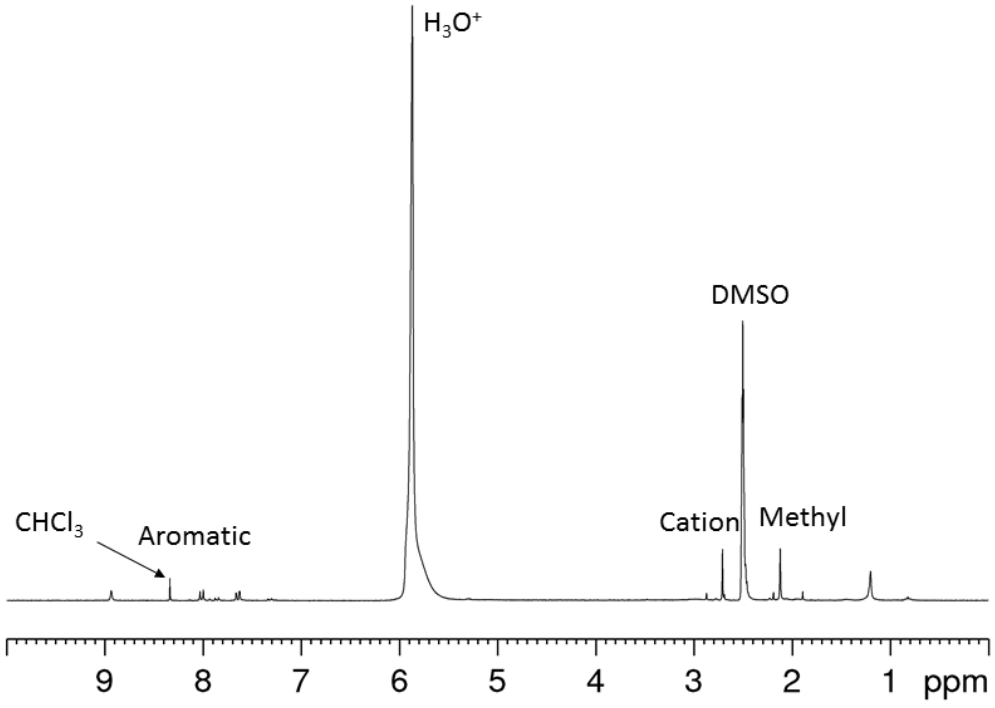

Figure 6 – Solution phase ^1H NMR spectrum of the 75% amide modified MOF $(Me_2NH_2)[In(BDC\text{-}NHC(O)CH_3)_{1.5}(ABDC)_{0.5}]$ (**75%AM**) after digestion

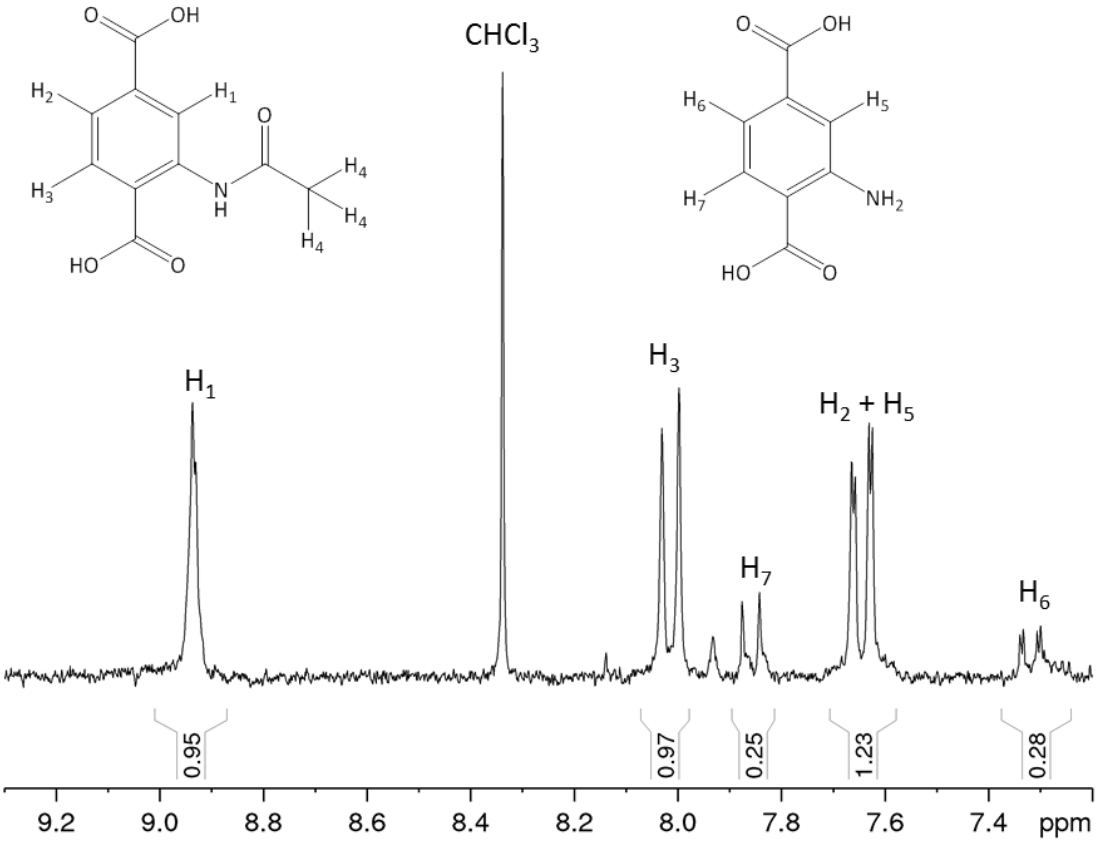

Figure 7 – Expanded range of the solution phase ^{1}H NMR spectrum of the 75% amide-modified MOF $(Me_2NH_2)[In(BDC\text{-}NHC(O)CH_3)_{1.5}(ABDC)_{0.5}]$ (**75%AM**) after digestion

NMR spectroscopy of 100% amide-modified MOF

A solution-phase ^{1}H NMR spectrum of the framework after the post-synthetic modification method B (**100%AM**) was obtained following the digestion procedure described in Section 5.3.3 (Figure 8). The proton environments suggest a full conversion of the organic ligand. An expanded section between 7.5 – 9.2 ppm is shown in Figure 9

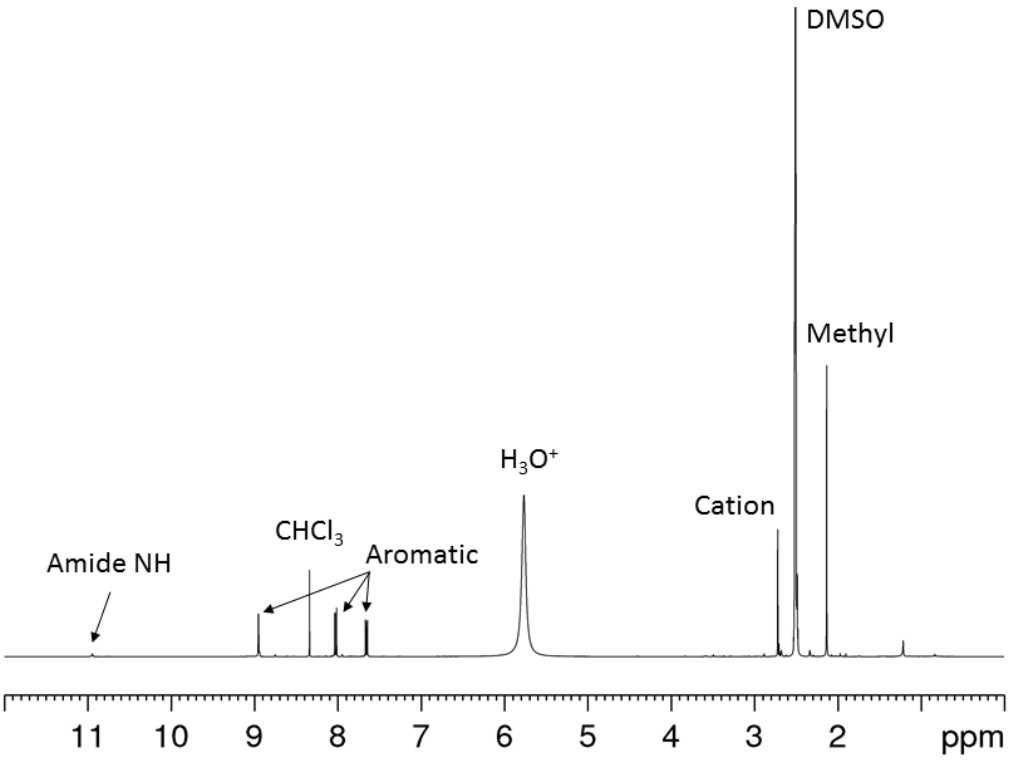

Figure 8 – Solution phase ^{1}H NMR spectrum of the 100% amide-modified MOF $(Me_2NH_2)[In(BDC\text{-}NHC(O)CH_3)_2]$ (**100%AM**) after digestion

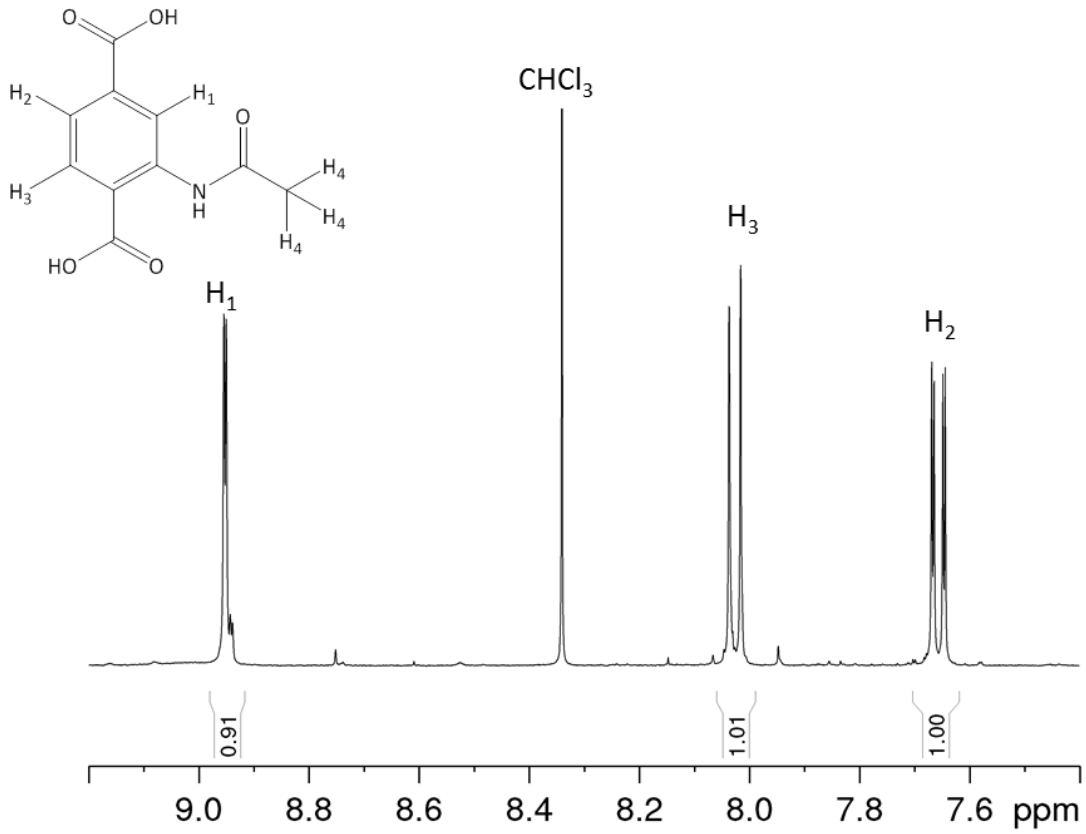

Figure 9 – Expanded range of the solution phase ^{1}H NMR spectrum of the 100% amide-modified MOF $(Me_2NH_2)[In(BDC\text{-}NHC(O)CH_3)_2]$ (**100%AM**) after digestion

Solid-state IR spectroscopy

A solid-state IR spectrum was collected for the 100% amide-modified MOF (**100%AM**). The spectrum is shown in Figure 10 in comparison to the IR spectrum of the as-synthesised parent MOF previously presented in Chapter 2.

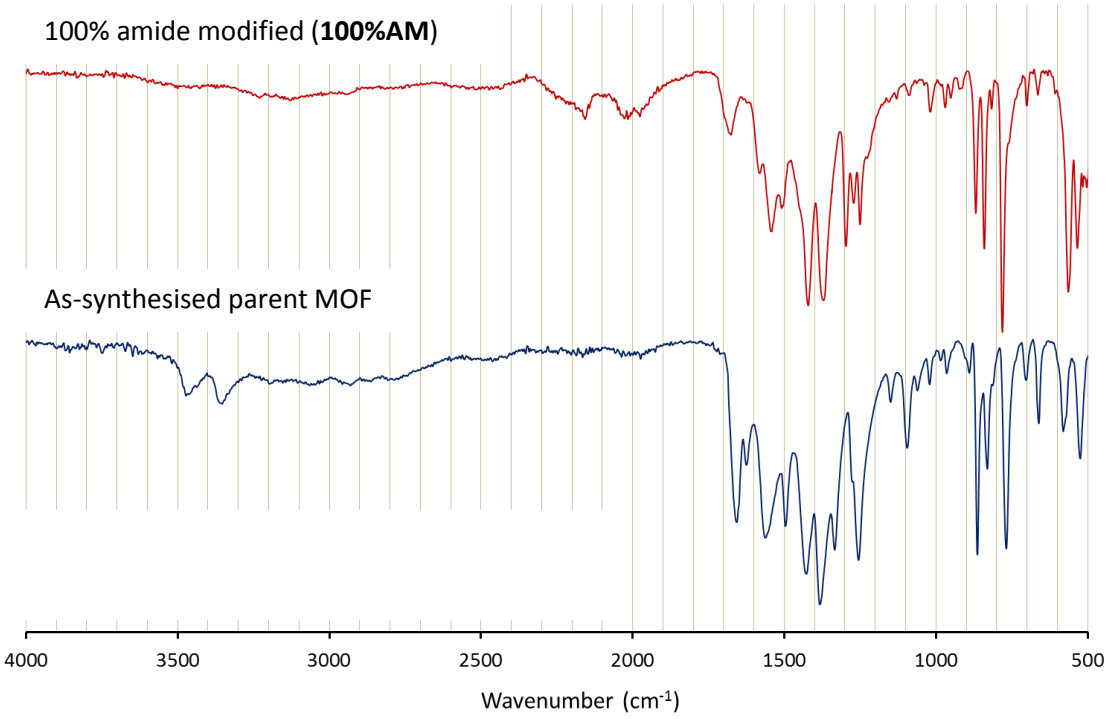

Figure 10 - Solid state IR spectra recorded for as-synthesised parent MOF $(Me_2NH_2)[In(ABDC)_2]$ (blue) and the 100% amide-modified MOF $(Me_2NH_2)[In(BDC\text{-}NHC(O)CH_3)_2]$ (**100%AM**) (red)

5.3.6 Crystallographic studies of desolvation of 100% amide-modified MOF $(Me_2NH_2)[In(BDC\text{-}NHC(O)CH_3)_2]$ using *in situ* heating

100% amide-modified MOF in $CHCl_3$ (**100%AM**)

The crystals of **100%AM** used for the *in situ* heating experiments were selected while still immersed in $CHCl_3$ and one face of the crystal was glued to a glass fibre while the crystal was still covered in a thin layer of residual solvent. Care was taken to avoid coating the entire crystal in adhesive. The crystal was rapidly transferred to the diffractometer and situated in the nitrogen stream of the Cryostream device at room temperature. The glue was left to dry for 15 mins before any data were collected. Heating was carried out *in situ* using the Cryostream device. A ramp rate of 4 °C/min was used to raise the temperature, which was held at the final value for a fixed period (see Table 4) before cooling at a ramp rate of 4 °C/min. Intensity data collections were recorded under the nitrogen stream at 298 K, using the Cryostream to maintain the temperature. Two different heating experiments were carried out on two separate crystals (**MH1** and **MH2**). The unit cell parameters were obtained by analysing reflections of $I/\sigma > 10$ from 4 sets of 10° omega scans with 0.5° slicing. A full data collection was recorded at the end of the study (**MH1.3**) and details are provided in Table 6.

Table 4 - Parameters used and unit cell determined for crystallographic studies of desolvation by *in situ* heating of 100% amide-modified MOF $(Me_2NH_2)[In(BDC\text{-}NHC(O)CH_3)_2]$ (**100%AM**)

Heating Study	Temp heated	Hold time at max. temp.	Data Set Code	*a* (Å)	*b* (Å)	*c* (Å)	*V* (Å^3)
MH1	25 °C	Start	**MH1.1**	14.518(5)	27.525(7)	31.264(6)	12493(6)
	80 °C	5 mins	**MH1.2**	14.44(1)	27.18(1)	31.55(1)	12379(11)
	150 °C		**MH1.3**	13.6375(7)	25.6631(13)	32.9087(16)	11517.4(10)
MH2	25 °C	Start	**MH2.1**	14.453(4)	27.039(9)	31.620(8)	12357(6)
	150 °C	5 mins	**MH2.2**	13.80(2)	25.89(3)	32.65(3)	11670(20)

All data collected at 298 K

100% amide-modified MOF after solvent exchange for DMF (**100%AM.DMF**)

The crystal of **100%AM.DMF** used for the *in situ* heating experiment was selected while still immersed in DMF and one face of the crystal was glued to a glass fibre while the crystal was still covered in a thin layer of residual solvent. Care was taken to avoid coating the entire crystal in adhesive. The crystal was rapidly transferred to the diffractometer and situated in the nitrogen stream of the Cryostream device at room temperature. The glue was left to dry for 15 mins before any data were collected. Heating was carried out *in situ* using the Cryostream device. A ramp rate of 4 °C/min was used to raise the temperature, which was held at the final value for a fixed period (see Table 5) before cooling at a ramp rate of 4 °C/min. Intensity data collections were recorded under the nitrogen stream at 298 K, using the Cryostream to maintain the temperature. The unit cell parameters were obtained by analysing reflections of I/σ > 10 from 4 sets of 10° omega scans with 0.5° slicing. A full data collection was recorded at the end of the study (**MH3.3**) and details are provided in Table 6.

Table 5 - Parameters used and unit cell determined for crystallographic studies of desolvation by *in situ* heating of 100% amide-modified MOF $(Me_2NH_2)[In(BDC\text{-}NHC(O)CH_3)_2]$ solvent-exchanged for DMF

Heating Study	Temp heated	Hold time	Data Set Code	*a* (Å)	*b* (Å)	*c* (Å)	*V* (Å^3)
MH3	25 °C	Start	**MH3.1**	14.715(4)	26.092(9)	32.283(7)	12395(6)
	150 °C	5 mins	**MH3.2**	14.497(8)	25.74(2)	32.58(1)	12159(11)
	150 °C	15 mins	**MH3.3**	13.8452(17)	25.667(3)	32.873(4)	11682(2)

All data collected at 298 K

5.3.7 Crystallographic studies of desolvation of 100% amide modified MOF $(Me_2NH_2)[In(BDC\text{-}NHC(O)CH_3)_2]$ using *ex situ* heating

A crystal of DMF-exchanged 100% amide-modified MOF (**100%AM.DMF**) was transferred from the DMF solvent to a microscope slide and left until the DMF had evaporated. The crystals were then heated in a temperature-controlled oven at 150 °C for 15 minutes. After the treatment the crystals were covered in perfluoropolyether oil (FOMBLIN Y) and one was mounted on a goniometer head. X-Ray diffraction data were recorded at 100 K (**MH4**). The temperature was maintained using a nitrogen Cryostream stream. The crystal retained most of its crystallinity, enabling detailed structural information to be obtained. Full crystallographic information for the structure is listed in Table 6.

Table 6 - Data collection, structure solution and refinement parameters for single crystal X-ray structure determinations of Heating experiments on 100% amide-modified MOF $(Me_2NH_2)[In(BDC\text{-}NHC(O)CH_3)_2]$

	In situ heating experiment **MH1** on 100% amide-modified MOF ($CHCl_3$) **(MH1.3)**	*In situ* heating experiment **MH3** on 100% amide-modified MOF (DMF) **(MH3.3)**	*Ex situ* heating experiment on 100% amide-modified MOF (DMF) **(MH4)**
Crystal Habit	Octahedron	Octahedron	Octahedron
Crystal Colour	Brown	Brown	Brown
Crystal Size (mm)	0.20 × 0.20 × 0.10	0.25 × 0.20 × 0.12	0.30 × 0.30 × 0.30
Crystal System	Orthorhombic	Orthorhombic	Orthorhombic
Space Group, Z	*Fddd*, 16	*Fddd*, 16	*Fddd*, 16
a (Å)	13.6375(7)	13.8452(17)	13.4004(5)
b (Å)	25.6631(13)	25.667(3)	25.0116(11)
c (Å)	32.9087(16)	32.873(4)	33.4655(13)
α (°)	90	90	90
β (°)	90	90	90
γ (°)	90	90	90
V (Å^3)	11517.4(10)	11682(2)	11216.5(8)
Radiation	Cu-K_α (λ = 1.54178 Å)	Cu-K_α (λ = 1.54178 Å)	Cu-K_α (λ = 1.54178 Å)
Density (g cm^{-3})[b]	1.392	1.372	1.429
Temperature (K)	298	298	100
μ (mm^{-1})[c]	6.997	6.791	7.210
2θ Range (°)	12.1 to 133.48	7.74 to 101.37	7.94 to 133.40
Reflns collected	21218	5595	7063
Independent reflns (R_{int})	2540 (0.0598)	1432 (0.0556)	2294 (0.0299)
Reflns used in refinement, *n*	2540	1432	2294
L.S. parameters, *p*	128	116	132
No. of restraints, *r*	15	10	23
Completeness	0.991	0.922	0.919
$R1(F)$[a] $I > 2\sigma(I)$	0.0949	0.1006	0.1017
$wR2(F^2)$[a], all data	0.2290	0.3241	0.2314
$S(F^2)$[a], all data	1.120	1.132	1.267

[a] $R1(F) = \sum(|F_o| - |F_c|)/\sum|F_o|$; $wR2(F^2) = \sqrt{\sum w\left(F_o^2 - F_c^2\right)^2/\sum wF_o^4}$; $S(F^2) = \sqrt{\sum w\left(F_o^2 - F_c^2\right)^2/(n+r-p)}$.

[b] Densities are calculated using only framework atoms and cations, and do not include guest molecules.

[c] Adsorption coefficients are calculated based on the crystallographic model

5.3.8 *In situ* crystallographic studies of CO_2 sorption in 100% amide-modified MOF $(Me_2NH_2)[In(BDC\text{-}NHC(O)CH_3)_2]$

Single Crystal diffraction experiment on the DMF-exchanged 100% amide-modified MOF (**MI1**)

Single crystals of DMF exchanged 100% amide modified MOF (**100%AM.DMF**) were removed from the DMF mother-liquor, dried in air for 15 minutes, and heated to 150 ^oC in a temperature controlled oven. The sample was held at 150 ^oC for 15 minutes and the removed from the oven while still at 150^oC. A crystal was then chosen and mounted in the I19 gas cell as detailed in section 5.3.2, the process took 15 minutes during which time the crystal was exposed to air. The sample was then placed under vacuum and an initial data collection was recorded (**MI1.1**). Successive pressures of CO_2 were then introduced at 1 bar, 5 bar , 10 bar and 20 bar allowing 30 minutes for equilibration at each pressure before recording diffraction data (**MI1.2 – MI1.5**). Full structure solutions were obtained as detailed in section 5.3.2. Table 7 shows the refined unit cell parameters during the study and Table 8 and Table 9 lists the full crystallographic information. All data were recorded at 298 K.

Table 7 - Unit cell parameters determined during crystallographic studies of CO_2 uptake in DMF-exchanged 100% amide-modified MOF $(Me_2NH_2)[In(BDC\text{-}NHC(O)CH_3)_2]$ (**MI1**)

Sample Description	Data set Code	*a* (Å)	*b* (Å)	*c* (Å)	*V* (Å^3)
Vacuum after heat treatment	**MI1.1**	14.1465(15)	25.9410(12)	32.8343(10)	12049.4(15)
1 bar CO_2	**MI1.2**	14.6331(5)	26.6688(12)	32.0891(9)	12522.7(8)
5 bar CO_2	**MI1.3**	14.6980(4)	26.9928(11)	31.7858(8)	12610.7(7)
10 bar CO_2	**MI1.4**	14.7157(4)	27.1498(11)	31.6408(8)	12641.4(7)
20 bar CO_2	**MI1.5**	14.7465(6)	27.3385(13)	31.4894(11)	12694.9(9)

Table 8 - Data collection, structure solution and refinement parameters for single crystal X-ray structure determinations of in situ crystallographic experiment **MI1** on 100% amide-modified MOF $(Me_2NH_2)[In(BDC\text{-}NHC(O)CH_3)_2]$ (**100%AM.DMF**)

	In situ CO_2 uptake of **100%AM.DMF**- Vacuum **(MI1.1)**	*In situ* CO_2 uptake of **100%AM.DMF**- 1 bar CO_2 **(MI1.2)**	*In situ* CO_2 uptake of **100%AM.DMF**- 5 bar CO_2 **(MI1.3)**
Crystal Habit	Octahedron	Octahedron	Octahedron
Crystal Colour	Brown	Brown	Brown
Crystal Size (mm)	0.2 × 0.15 × 0.15	0.2 × 0.15 × 0.15	0.2 × 0.15 × 0.15
Crystal System	Orthorhombic	Orthorhombic	Orthorhombic
Space Group, Z	*Fddd*, 16	*Fddd*, 16	*Fddd*, 16
a (Å)	14.1465(15)	14.6331(5)	14.6980(4)
b (Å)	25.9410(12)	26.6688(12)	26.9928(11)
c (Å)	32.8343(10)	32.0891(9)	31.7858(8)
α (°)	90	90	90
β (°)	90	90	90
γ (°)	90	90	90
V (Å^3)	12049.4(15)	12522.7(8)	12610.7(7)
Radiation	Synchrotron (λ = 0.6889 Å)	Synchrotron (λ = 0.6889 Å)	Synchrotron (λ = 0.6889 Å)
Density (g cm^{-3})[b]	1.331	1.280	1.271
Temperature (K)	298	298	298
μ (mm^{-1})[c]	0.773	0.744	0.731
2θ Range (°)	3.40 to 48.41	3.32 to 53.14	3.30 to 53.14
Reflns collected	17224	22487	22898
Independent reflns (R_{int})	2662 (0.0872)	3580 (0.0844)	3603 (0.0824)
Reflns used in refinement, *n*	2662	3580	3603
L.S. parameters, *p*	118	157	159
No. of restraints, *r*	14	3	3
Completeness	0.997	0.994	0.995
$R1(F)$[a] $I > 2\sigma(I)$	0.1072	0.0813	0.0803
$wR2(F^2)$[a], all data	0.3403	0.2517	0.2549
$S(F^2)$[a], all data	1.383	1.086	1.100

[a] $R1(F) = \sum(|F_o| - |F_c|)/\sum|F_o|$; $wR2(F^2) = \sqrt{\sum w\left(F_o^2 - F_c^2\right)^2/\sum wF_o^4}$; $S(F^2) = \sqrt{\sum w\left(F_o^2 - F_c^2\right)^2/(n+r-p)}$.

[b] Densities are calculated using only framework atoms and cations, and do not include guest molecules.

[c] Adsorption coefficients are calculated based on the crystallographic model

Table 9 - Data collection, structure solution and refinement parameters for single crystal X-ray structure determinations of in situ crystallographic experiment **MI1** on 100% amide-modified MOF $(Me_2NH_2)[In(BDC\text{-}NHC(O)CH_3)_2]$

	In situ CO_2 uptake of **100%AM.DMF -** 10 bar CO_2 **(MI1.4)**	*In situ* CO_2 uptake of **100%AM.DMF**- 20 bar CO_2 **(MI1.5)**
Crystal Habit	Octahedron	Octahedron
Crystal Colour	Brown	Brown
Crystal Size (mm)	0.2 × 0.15 × 0.15	0.2 × 0.15 × 0.15
Crystal System	Orthorhombic	Orthorhombic
Space Group, Z	*Fddd*, 16	*Fddd*, 16
a (Å)	14.7157(4)	14.7465(6)
b (Å)	27.1498(11)	27.3385(13)
c (Å)	31.6408(8)	31.4894(11)
α (°)	90	90
β (°)	90	90
γ (°)	90	90
V (Å^3)	12641.4(7)	12694.9(9)
Radiation	Synchrotron (λ = 0.6889 Å)	Synchrotron (λ = 0.6889 Å)
Density (g cm^{-3})[b]	1.268	1.263
Temperature (K)	298	298
μ (mm^{-1})[c]	0.737	0.731
2θ Range (°)	3.30 to 53.14	3.28 to 48.42
Reflns collected	22896	19397
Independent reflns (R_{int})	3606 (0.0802)	2820 (0.0780)
Reflns used in refinement, *n*	3606	2820
L.S. parameters, *p*	159	135
No. of restraints, *r*	3	13
Completeness	0.995	1.000
$R1(F)$[a] $I > 2\sigma(I)$	0.0873	0.0876
$wR2(F^2)$[a], all data	0.2706	0.2780
$S(F^2)$[a], all data	1.097	1.077

[a] $R1(F) = \sum(|F_o| - |F_c|)/\sum|F_o|$; $wR2(F^2) = \sqrt{\sum w\left(F_o^2 - F_c^2\right)^2/\sum wF_o^4}$; $S(F^2) = \sqrt{\sum w\left(F_o^2 - F_c^2\right)^2/(n+r-p)}$.

[b] Densities are calculated using only framework atoms and cations, and do not include guest molecules.

[c] Adsorption coefficients are calculated based on the crystallographic model

Powder diffraction on a $CHCl_3$-containing 100% amide-modified MOF (**MI2**)

A powdered sample of 100% amide modified MOF $(Me_2NH_2)[In(BDC\text{-}NHC(O)CH_3)_2]$ (**100%AM**) was packed into a 0.5 mm quartz capillary and fixed into the I11 gas cell using araldite adhesive. The sample was placed under dynamic vacuum (≈10^{-5} mbar) for 8 hours before collecting a powder pattern on the I11 beamline (**MI2.1**), λ = 0.82665(5) Å.[33, 34] The sample was then loaded with successive pressures of CO_2 at 1 bar, 3 bar, 5 bar, 10 bar and 20 bar, and allowed to equilibrate for 30 mins before collected powder patterns (**MI2.2 – MI2.6**). The powder patterns are displayed in Figure 11 and the unit cell values from Pawley refinements are shown in Table 10. All data was recorded at room temperature.

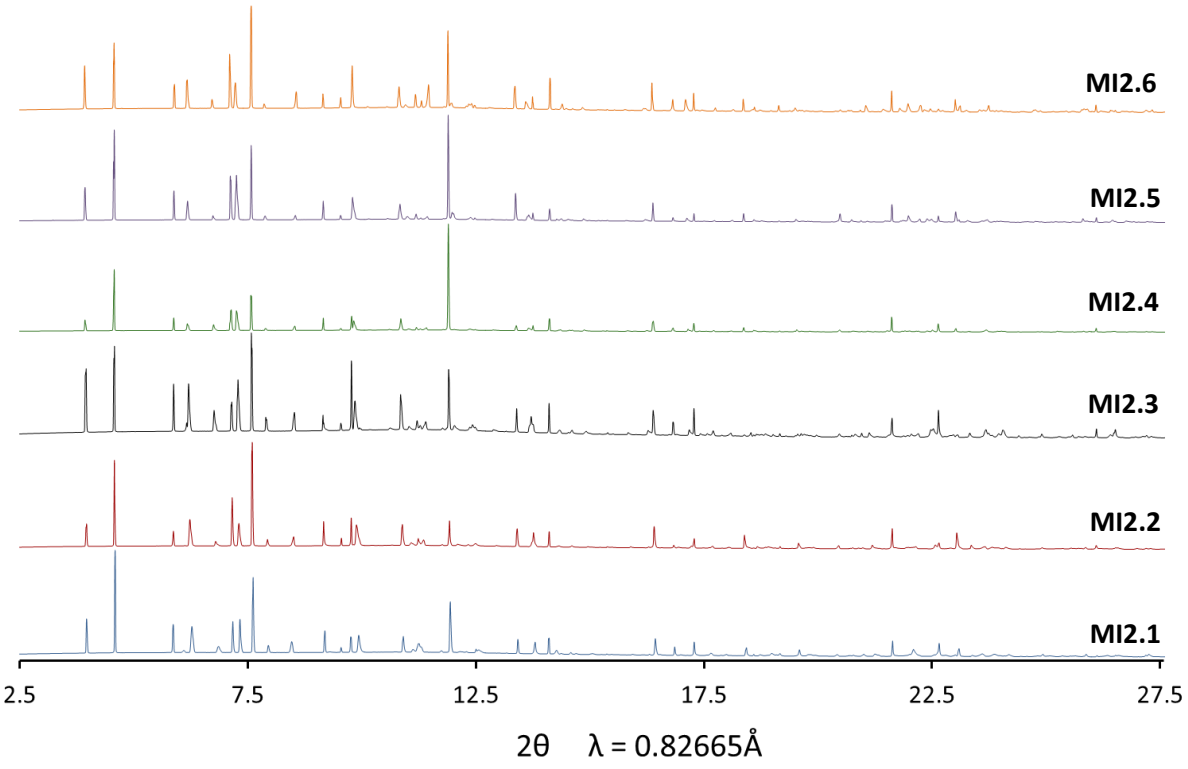

Figure 11 - Powder diffraction patterns obtained during *in situ* crystallographic CO_2 uptake experiment **MI2** on 100% amide-modified MOF $(Me_2NH_2)[In(BDC\text{-}NHC(O)CH_3)_2]$ (**100%AM**)

Table 10 - Unit cell parameters determined during crystallographic studies of CO_2 uptake in 100% amide-modified MOF $(Me_2NH_2)[In(BDC\text{-}NHC(O)CH_3)_2]$ (**MI2**)

Sample Description	Data set Code	*a* (Å)	*b* (Å)	*c* (Å)	*V* (Å^3)
Vacuum	**MI2.1**	14.6046(6)	27.616(1)	31.075(1)	12533.2(8)
1 bar CO_2	**MI2.2**	14.6416(4)	27.827(1)	30.893(1)	12586.9(7)
3 bar CO_2	**MI2.3**	14.6878(4)	27.9525(9)	30.780(1)	12637.2(7)
5 bar CO_2	**MI2.4**	14.7227(3)	28.0336(8)	30.6965(8)	12669.4(6)
10 bar CO_2	**MI2.5**	14.7557(3)	28.1050(7)	30.6254(7)	12700.6(5)
20 bar CO_2	**MI2.6**	14.8068(3)	28.2032(6)	30.5423(6)	12754.5(5)

The unit cell of the MOF was initially determined by analysis of the positions of the first few Bragg reflections and their known Miller indices. These unit cell parameters were used as a starting point for Pawley[37] refinements. Representative fits for vacuum (**MI2.1**) and 20 bar (**MI2.6**) are detailed below. The fitting is poor due to obvious splitting of the peaks. Many of these peaks however only correspond to one set of Miller indices in the Pawley fit. This is thought to occur due to a combination of closely related phases which were not modelled in the fitting and will be covered in detail in section 5.4.3.

The single-phase refinement of **MI2.1** employed 995 parameters (12 background, 1 zero error, 5 profile, 3 cell and 974 reflections), resulting in final indices of fit R_{wp} = 9.364, $R_{wp'}$ = 29.302. The final unit cell parameters were orthorhombic *a* = 14.6046 (6) Å, *b* = 27.616 (1) Å, *c* = 31.075 (1) Å, *V* = 12533.2 (8) Å^3. The fit is displayed in Figure 12

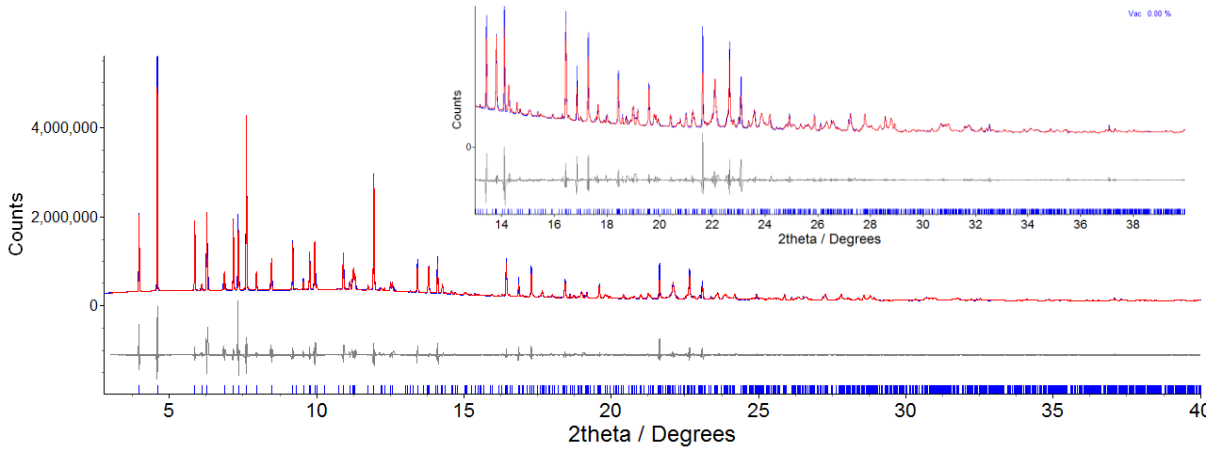

Figure 12 – Observed (blue) and calculated (red) and difference plot [I_{obs} - I_{calc}] (grey) of the Pawley[37] refinement of 100% amide-modified MOF $(Me_2NH_2)[In(BDC\text{-}NHC(O)CH_3)_2]$ under vacuum (**MI2.1**) (2θ range 3.0 – 40.0 °, d_{min} = 1.2 Å).

The single phase refinement of **MI2.5** employed 1,017 parameters (12 background, 1 zero error, 5 profile, 3 cell and 984 reflections), resulting in final indices of fit R_{wp} = 9.755, $R_{wp'}$ = 29.119. The final unit cell parameters were orthorhombic a = 14.8068(3) Å, b = 28.2032(6) Å, c = 30.5423(6) Å, V = 12754.5(5) Å^3. The fit is displayed in Figure 13

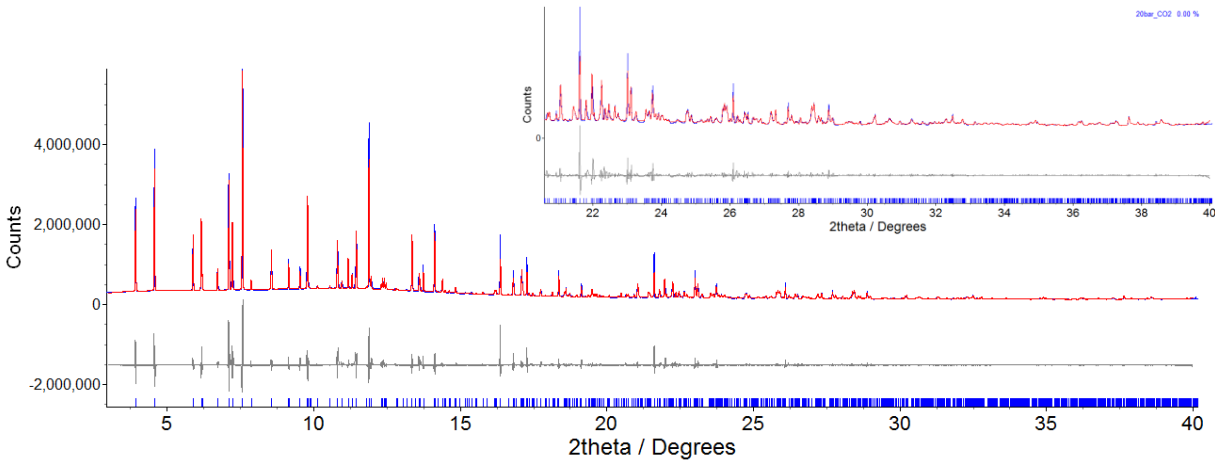

Figure 13 – Observed (blue) and calculated (red) and difference plot [I_{obs} - I_{calc}] (grey) of the Pawley[37] refinement 100% amide modified MOF $(Me_2NH_2)[In(BDC\text{-}NHC(O)CH_3)_2]$ under 20 bar CO_2 (**MI2.5**) (2θ range 3.0 – 40.0 °, d_{min} = 1.2Å).

5.3.9 Crystallographic characterisation after cation exchange reactions of $(Me_2NH_2)[In(ABDC)_2]$

Post-synthetic cation exchange reactions were carried out on $(Me_2NH_2)[In(ABDC)_2]$ via the three synthetic methods (A-C) described in section 5.3.2 (**AgM**). The reactions involved exchange of the dimethyl ammonium cation with Ag^+ ions. The single crystals obtained after PSM reactions were directly transferred into a perfluoropolyether oil (FOMBLIN Y). The crystals were mounted onto a MiTeGen 200µm MicroMount under an optical microscope, and transferred to the diffractometer where the crystal was immersed in the dry nitrogen stream of the Crysotream device at 100 K. Table 11 lists the crystal structures obtained and the relative occupancies of the Ag^+ ions in the crystallographic model (**S1-5**). The cation exchange percentage is double the refined crystallographic occupancy value as the asymmetric unit contains only half a cation. Full refinement parameters can be seen in Table 12 and Table 13. In all cases the Ag^+ ion was initially modelled anisotropically with a refinable partial occupancy. In crystals **S2** and **S3** this, however, resulted in reasonably large residual election density peaks (3 - 5 e^- / $Å^3$) within 1 Å of the modelled Ag. A crystallographic model of the Ag^+ disordered over several locations was therefore also attempted. This resulted in an overall increase in the occupancy and therefore the cation exchange percentage.

Table 11 - Modification details and cation exchange percentage based on refined chemical occupancies obtained from single crystal X-ray structure determinations of Ag^+ ion-exchanged MOF $(Me_2NH_2)_{(1-x)}Ag_x[In(ABDC)_2]$

Crystal Code	Modification Details	Ag^+ ion occupancy modelled anisotropically as a single site (modelled disordered over 4 isotropic sites)
S1	Method A	24%
S2		26% (40%)
S3	Method B	30% (35%)
S4	Method C	27%
S5		33%

5.3.10 Crystallographic studies of desolvation of Ag^+ ion-exchanged $(Me_2NH_2)_{(1-x)}Ag_x[In(ABDC)_2]$ using *ex situ* heating

A crystal of Ag^+ ion-exchanged MOF $(Me_2NH_2)_{(1-x)}Ag_x[In(ABDC)_2]$ (**AgM**) was transferred from the DMF solvent to a microscope slide and left until the residual DMF on the slide had evaporated. The crystals were then heated in a temperature controlled oven at 100 ^oC for 10 minutes. After the treatment the crystals were covered in a perfluoropolyether oil (FOMBLIN Y) and one was mounted on a goniometer head. X-Ray diffraction data were recorded at reduced temperatures (100K) under a cold nitrogen stream (**SH1**). The procedure above was carried out in the dark to avoid photodegradation. The crystal retained some crystallinity, but the resolution and completeness of the data was poor. A crystallographic model of the Ag^+ disordered over three locations was deemed the most appropriate and resulted in an overall occupancy of 27% within the asymmetric unit. This corresponds to a cation exchange of 54%. Full crystallographic information for the structure is listed in Table 13.

Table 12 - Data collection, structure solution and refinement parameters for single crystal X-ray structure determinations of Ag^+ ion-exchanged MOF $(Me_2NH_2)_{(1-x)}Ag_x[In(ABDC)_2]$

	Ag^+ ion-exchanged MOF (Method A) - 1 **(S1)**	Ag^+ ion-exchanged MOF (Method A) - 2 **(S2)**	Ag^+ ion-exchanged MOF (Method B) **(S3)**
Crystal Habit	Octahedron	Octahedron	Octahedron
Crystal Colour	Brown	Brown	Brown
Crystal Size (mm)	0.20 × 0.20 × 0.20	0.20 × 0.20 × 0.20	0.30 × 0.30 × 0.30
Crystal System	Orthorhombic	Orthorhombic	Orthorhombic
Space Group, Z	*Fddd*, 16	*Fddd*, 16	*Fddd*, 16
a (Å)	15.6552(8)	15.3038(3)	15.5097(4)
b (Å)	26.8662(9)	26.4113(7)	26.6818(6)
c (Å)	31.2384(10)	31.8700(7)	31.3856(7)
α (°)	90	90	90
β (°)	90	90	90
γ (°)	90	90	90
V (Å^3)	13138.7(9)	12881.7(5)	12988.2(5)
Radiation	Mo-K_α (λ = 0.71073 Å)	Synchrotron (λ = 0.6889 Å)	Mo-K_α (λ = 0.71073 Å)
Density (g cm^{-3})[b]	1.080	1.104	1.109
Temperature (K)	100	100	100
μ (mm^{-1})[c]	1.027	1.234	1.178
2θ Range (°)	6.54 to 50.698	3.228 to 51.006	3.302 to 55.188
Reflns collected	6573	44660	52779
Independent reflns (R_{int})	3003 (0.0295)	3287 (0.1081)	3780 (0.0219)
Reflns used in refinement, *n*	3003	3287	3780
L.S. parameters, *p*	148	113	139
No. of restraints, *r*	3	35	0
Completeness	0.997	0.997	0.999
$R1(F)$[a] $I > 2\sigma(I)$	0.0866	0.1330	0.0747
$wR2(F^2)$[a], all data	0.2846	0.3608	0.2731
$S(F^2)$[a], all data	1.101	1.229	1.182

[a] $R1(F) = \sum(|F_o| - |F_c|)/\sum|F_o|$; $wR2(F^2) = \sqrt{\sum w\left(F_o^2 - F_c^2\right)^2/\sum wF_o^4}$; $S(F^2) = \sqrt{\sum w\left(F_o^2 - F_c^2\right)^2/(n+r-p)}$.

[b] Densities are calculated using only framework atoms and cations, and do not include guest molecules.

[c] Adsorption coefficients are calculated based on the crystallographic model

Table 13 - Data collection, structure solution and refinement parameters for single crystal X-ray structure determinations of of Ag^+ ion-exchanged MOF $(Me_2NH_2)_{(1-x)}Ag_x[In(ABDC)_2]$

	Ag^+ ion-exchanged MOF (Method C) - 1 **(S4)**	Ag^+ ion-exchanged MOF (Method C) - 2 **(S5)**	*Ex situ* heating experiment on Ag^+ ion-exchanged MOF **(SH1)**
Crystal Habit	Octahedron	Octahedron	Octahedron
Crystal Colour	Brown	Brown	Brown
Crystal Size (mm)	0.4 × 0.3 × 0.2	0.18 × 0.18 × 0.1	0.32 × 0.2 × 0.17
Crystal System	Orthorhombic	Orthorhombic	Orthorhombic
Space Group, Z	*Fddd*, 16	*Fddd*, 16	*Fddd*, 16
a (Å)	15.5040(11)	15.4682(13)	14.974(6)
b (Å)	26.6716(19)	26.659(2)	25.598(10)
c (Å)	31.457(2)	31.480(3)	32.336(12)
α (°)	90	90	90
β (°)	90	90	90
γ (°)	90	90	90
V (Å^3)	13007.9(16)	12981.3(19)	12395(8)
Radiation	Mo-K_α (λ = 0.71073 Å)	Mo-K_α (λ = 0.71073 Å)	Mo-K_α (λ = 0.71073 Å)
Density (g cm^{-3})[b]	1.106	1.113	1.185
Temperature (K)	110	100	100
μ (mm^{-1})[c]	1.068	1.130	1.411
2θ Range (°)	3.302 to 55.014	3.308 to 55.284	6.366 to 41.624
Reflns collected	23135	14221	2505
Independent reflns (R_{int})	3739 (0.0360)	3788 (0.0519)	1412 (0.0466)
Reflns used in refinement, *n*	3739	3788	1412
L.S. parameters, *p*	145	139	123
No. of restraints, *r*	3	1	4
Completeness	0.996	0.999	0.868
$R1(F)$[a] $I > 2\sigma(I)$	0.0891	0.0862	0.1016
$wR2(F^2)$[a], all data	0.3350	0.3003	0.3458
$S(F^2)$[a], all data	1.217	1.099	1.194

[a] $R1(F) = \sum(|F_o| - |F_c|)/\sum|F_o|$; $wR2(F^2) = \sqrt{\sum w\left(F_o^2 - F_c^2\right)^2/\sum wF_o^4}$; $S(F^2) = \sqrt{\sum w\left(F_o^2 - F_c^2\right)^2/(n+r-p)}$.

[b] Densities are calculated using only framework atoms and cations, and do not include guest molecules.

[c] Adsorption coefficients are calculated based on the crystallographic model

5.3.11 Bulk phase analysis of Ag^+ ion-exchanged $(Me_2NH_2)_{(1-x)}Ag_x[In(ABDC)_2]$

The phase purity of the Ag^+ ion-exchanged framework was confirmed through X-ray powder diffraction. A room temperature pattern (**PS1**) was collected at the I11 beamline[15, 16] as detailed in Section 5.3.3, λ = 0.82562(1) Å, after preparing the sample in a dark room. The unit cell parameters were initially determined by analysis of the positions of the first few Bragg reflections and their known Miller indices. These parameters were used as starting point for a Pawley refinement, employing 1,965 parameters (16 background, 1 zero error, 5 profile, 3 cell and 1,940 reflections), resulting in final indices of fit R_{wp} = 2.596, $R_{wp'}$ = 8.470. The final unit cell parameters were orthorhombic a = 15.6872 (2) Å, b = 26.6124 (4) Å, c = 31.4540 (5) Å, V = 13131.2 (3) $Å^3$. The fit is shown in Figure 14.

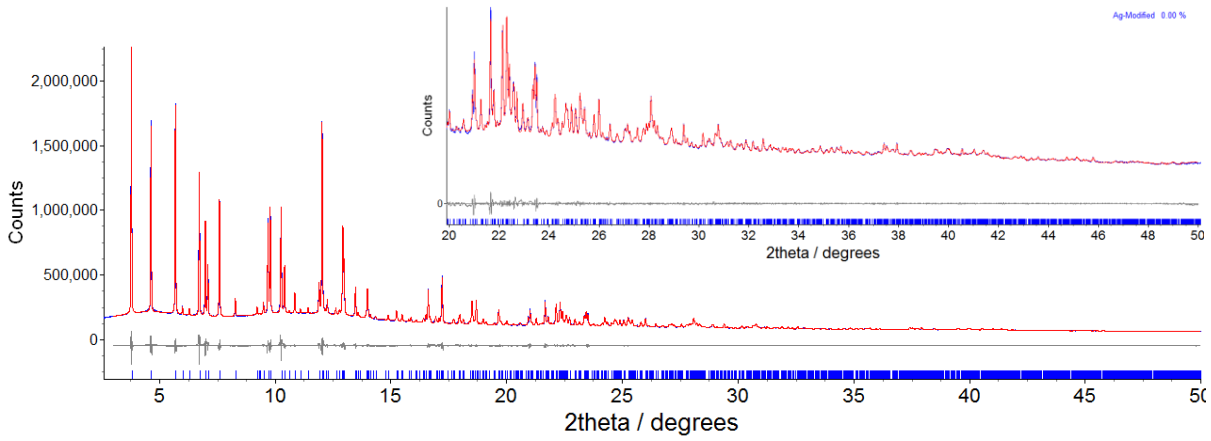

Figure 14 – Observed (blue) and calculated (red) and difference plot [I_{obs}-I_{calc}] (grey) of the Pawley[17] refinement of Ag^+ ion-exchanged MOF $(Me_2NH_2)_{(1-x)}Ag_x[In(ABDC)_2]$ **PS1** (2θ range 3.0 – 50.0 °, d_{min} = 0.97Å).

5.4 Results and discussion

5.4.1 Post-synthetic modification of the amino group in $(Me_2NH_2)[In(ABDC)_2]$ to a methyl amide.

Initial modification (75% conversion)

The initial modification reaction of the amine to a methyl amide (Method A, section 5.2.2) was carried out using $CHCl_3$ for the solvent, based on literature precedent from another framework.[19] The parent MOF is in an open-pore form when fully solvated in $CHCl_3$ therefore it is ideal for diffusion of reactants into the pores. The transformation occurred in a single crystal process allowing full structural analysis by X-ray diffraction (**M1**). The symmetry of the framework remained unchanged and was solved in space group *Fddd*. Evidence of the amide group was clearly present in the residual electron density and was able to be modelled using crystallographic restraints. The occupancy of the group was fixed at 75% and was stably refined with reasonable isotropic displacement parameters. This closely matched the integration of ^1H NMR peaks of the digested framework, which suggested an 80% conversion (section 5.4.8) (Figure 6). PSM reactions undergoing single crystal transitions have been reported before in IRMOF-3[41] and $[(ZnI_2)(TPT)_2(AmTP)]$ (TPT = tris(4-pyridyl)triazine, AmTP = aminotriphenylene),[42] but reports are relatively rare.[11] Furthermore the single crystal structure of modified IRMOF-3 only showed the location the framework atoms and not the new functional group, due to significant positional disorder, and the aminotriphenylene (AmTP) modified in $[(ZnI_2)(TPT)_2(AmTP)]$ is actually an immobilised guest molecule and not a modification of the framework itself.

The partial conversion seen is common among PSM reactions; the modification of UiO-66 with acetic anhydride using similar conditions achieved an 88% conversion,[19] and the first reported PSM reaction using IRMOF-3 occurred with an 80% conversion.[16] Quantitative conversions can, however be achieved, and have been published for both frameworks by adjusting the synthetic conditions.[18, 41]

The asymmetric unit of the modified MOF (shown in Figure 15) contained a 25% occupancy amine group on one position of the ring, and the 75% occupancy methyl amide on another position corresponding to an 180° rotation of the ring. The amide group displayed a slight wagging disorder which was crystallographically modelled but has been removed from the images for clarity.

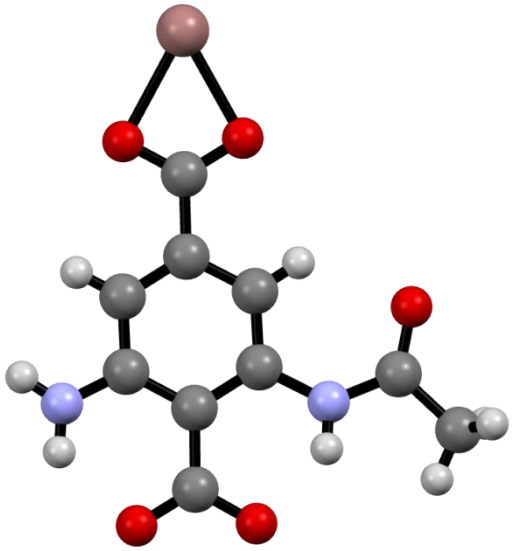

Figure 15 - Ball and Stick representation of the asymmetric unit in 75% amide-modified MOF $(Me_2NH_2)[In(BDC\text{-}NHC(O)CH_3)_{1.5}(ABDC)_{0.5}]$ (**M1**) Disorder of the amide group has been removed for clarity

The crystal structure displayed similar *b*- and *c*-axis lengths to the parent MOF, but a reduced *a*-axis. This resulted from maintenance of the overall pore shape but a slight contraction of the helical chains running parallel to the channel. The effect can be observed in Figure 16 a) and b) showing the modified and parent framework respectively. This was surprising considering the change in unit cell dimensions mainly occurs along the *a*-axis and the increased number of atoms would be expected to cause and increase in that dimension. Figure 16 c) shows the formation of a carbonyl – carbonyl interaction between neighbouring amide groups which may help stabilise the structure and be responsible for the contraction. The interaction combined with a change in steric requirements is likely to be responsible for difference in the position of the amide and amine groups. Similar structural analysis after PSM reactions is uncommon within the literature, due to the difficulties associated with determining accurate structural solutions from powder diffraction, and the potential for positional disorder often observed for the amide group.

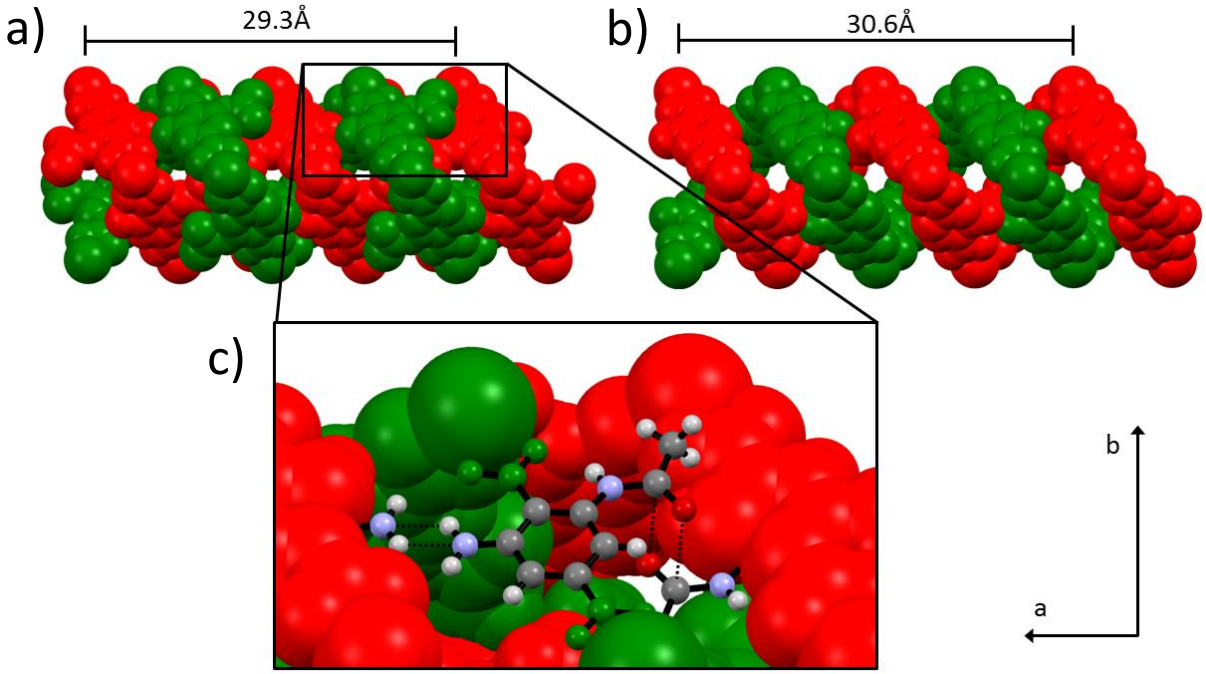

Figure 16 – Spacefill representation of a) 75% amide-modified MOF $(Me_2NH_2)[In(BDC\text{-}NHC(O)CH_3)_{1.5}(ABDC)_{0.5}]$ (**M1**) and b) as-synthesised MOF $(Me_2NH_2)[In(ABDC)_2]$ (**1**) viewed along the *c*-axis. c) View of the different amine and amide environments of **M1** and interactions occurring between neighbouring interpenetrated chains. Disorder of the amide group has been removed for clarity

Desolvation studies of the parent compound (**1-10**) showed a similar but smaller contraction of the helical chains (*a*-axis), which was largely ignored in discussion of the breathing effect, due to the flexibility being predominantly two-dimensional (*b*- and *c*-axes). The change in the *a*-axis due to the modification was ≈ 0.7 Å, larger than the entire breathing range of the parent compound (< 0.5 Å), despite the modified framework still remaining in the open-pore form. This resulted in a reasonable reduction in the unit volume which is illustrated in Figure 17, and a decrease in the solvent accessible void of 36% (calculated in comparison to crystal **1** using the solvent accessible void determined by the SQUEEZE routine in the program PLATON).[32]

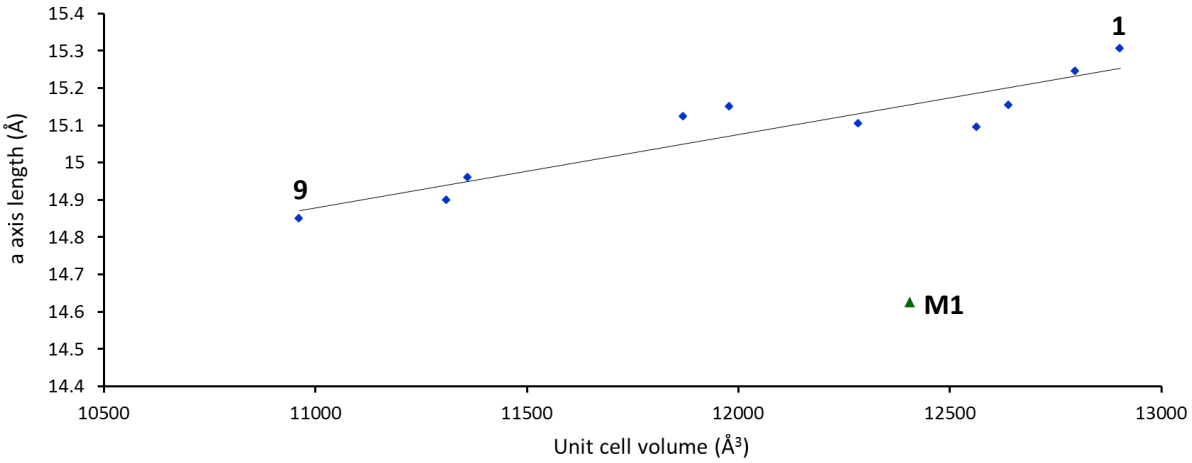

Figure 17 - *a*-axis and unit cell volume for 75% amide-modified MOF $(Me_2NH_2)[In(BDC\text{-}NHC(O)CH_3)_{1.5}(ABDC)_{0.5}]$ (green triangle) (**M1**) compared to desolvation studies on single crystals of as-synthesised parent MOF $(Me_2NH_2)[In(ABDC)_2]$ (blue diamonds) (**1-10**)

Full conversion

The PSM method was developed and by scaling up the reaction quantities, while maintaining the same solvent volume (Method B, section 5.2.2), a 100% amide-containing framework was able to be synthesised. The aromatic and methyl protons corresponding to the modified ligand in the digested NMR is shown in Figure 18.

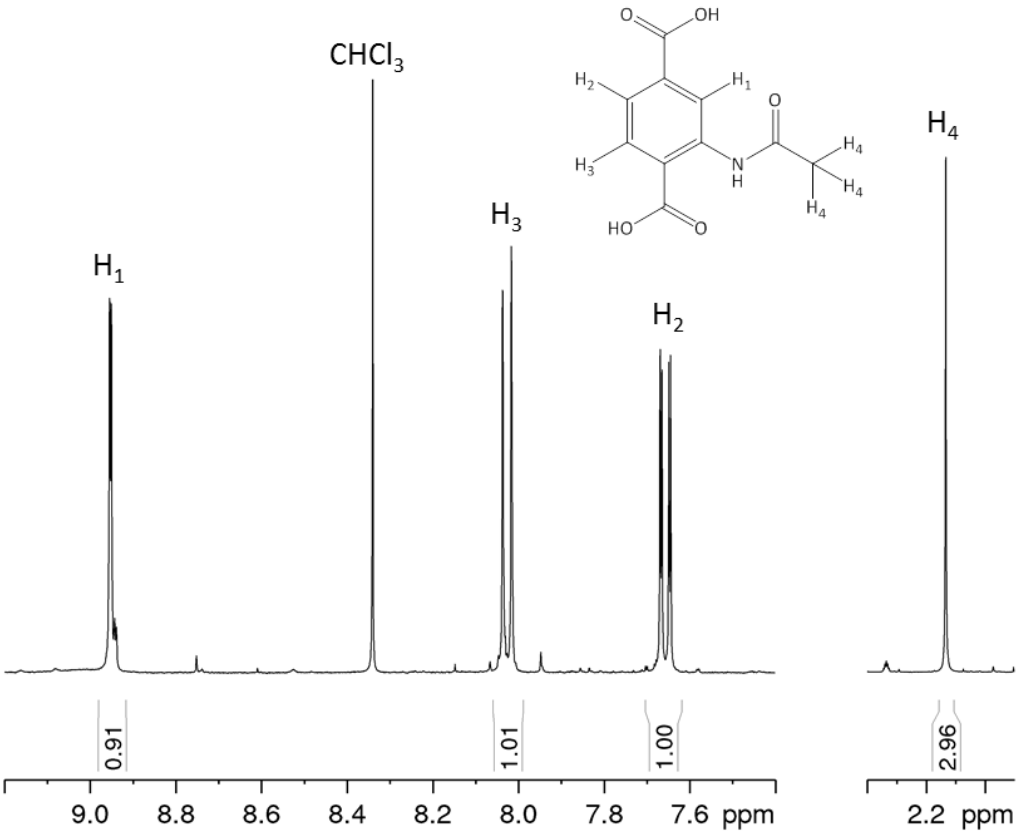

Figure 18 - Solution Phase NMR of the digestion components of 100% amide modified MOF (**100%AM**). Digestion was carried out using the procure detailed in section 5.3.3

The conversion also occurred in a single-crystal manner and structure determination by X-ray diffraction (**M2**) now showed a fully occupied amide group at only 1 site on the ring. A similar helical chain contraction to **M1** was also observed with the same carbonyl-carbonyl interaction between neighbouring amide groups. The quality of the diffraction data was high and allowed for location of the both the cation and the solvent contained in the pores. The disordered cation sat at the edges of the channels while the disordered $CHCl_3$ was modelled sitting directly in the middle of the channel. This is shown in Figure 19. The cation was seen to be in an ideal location to hydrogen bond to the amide oxygen.

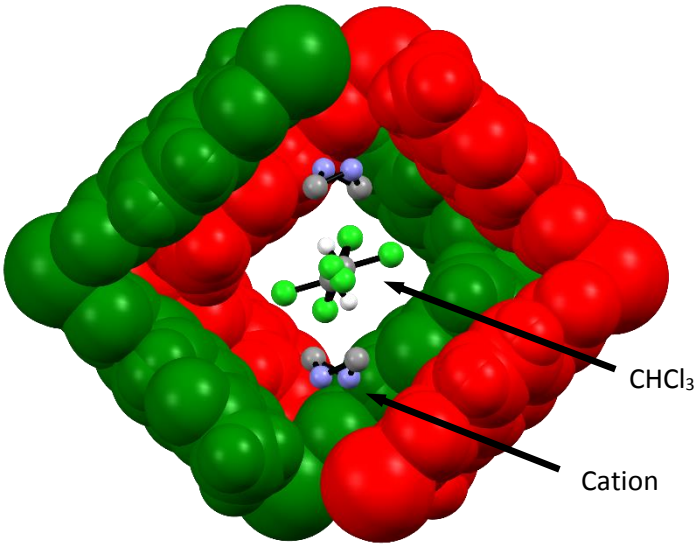

Figure 19 –Ball and stick representation of the contained cation and $CHCl_3$ solvent molecules, viewed down the *a*-axis showing one pore of 100% amide-modified MOF $(Me_2NH_2)[In(BDC\text{-}NHC(O)CH_3)_2]$ **M2**. Disorder on the framework has been removed for clarity

Solvent exchange

Single crystals of the modified MOF were able to be solvent exchanged with DMF in a SC-SC manner, and were analysed using X-ray diffraction (**M3**). The asymmetric unit of the DMF-containing framework was very similar to that of the $CHCl_3$-containing structure, displaying only one site for the amide group, cations on the edge of the channel and partially occupied disordered DMF molecules in the centre of the channels. The *b*- and *c*-axis lengths, however, were significantly different despite being recorded at the same temperature as the $CHCl_3$-containing MOF (**M2**). These are displayed in Figure 20 and show that the variations seem to follow the same breathing trend observed for the parent material.

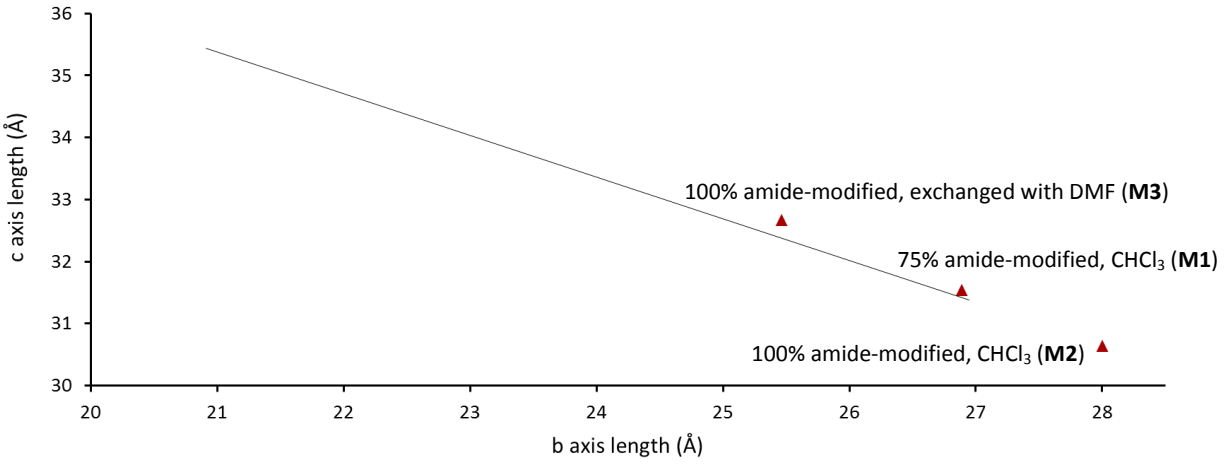

Figure 20 - *b*- and *c*-axis values of single crystal structures **M1-3** in comparison to the trend from single crystal desolvation studies of as-synthesised $(Me_2NH_2)[In(ABDC)_2]$ (**1-10**)

Powder diffraction analysis

Bulk sample analysis of the fully modified framework was carried out through X-ray powder diffraction. A comparison of the recorded diffraction pattern for the $CHCl_3$-containing sample (**PM1**) to the calculated pattern from the corresponding single crystal structure **M2** is shown in Figure 21. This displays a good qualitative match and combined with the digested NMR analysis confirms that the modification has occurred throughout the whole sample while maintaining the framework structure and the crystallinity. This was also confirmed in the DMF-exchanged framework (**PM2**) by a Rietveld[40] refinement using the framework atoms of **M3** as a starting point (Figure 5). The position and orientations of the cation and solvent molecules (modelled as rigid bodies) were optimised during the refinement by simulated annealing, but minimised to a location very similar to those modelled in the single crystal structure.

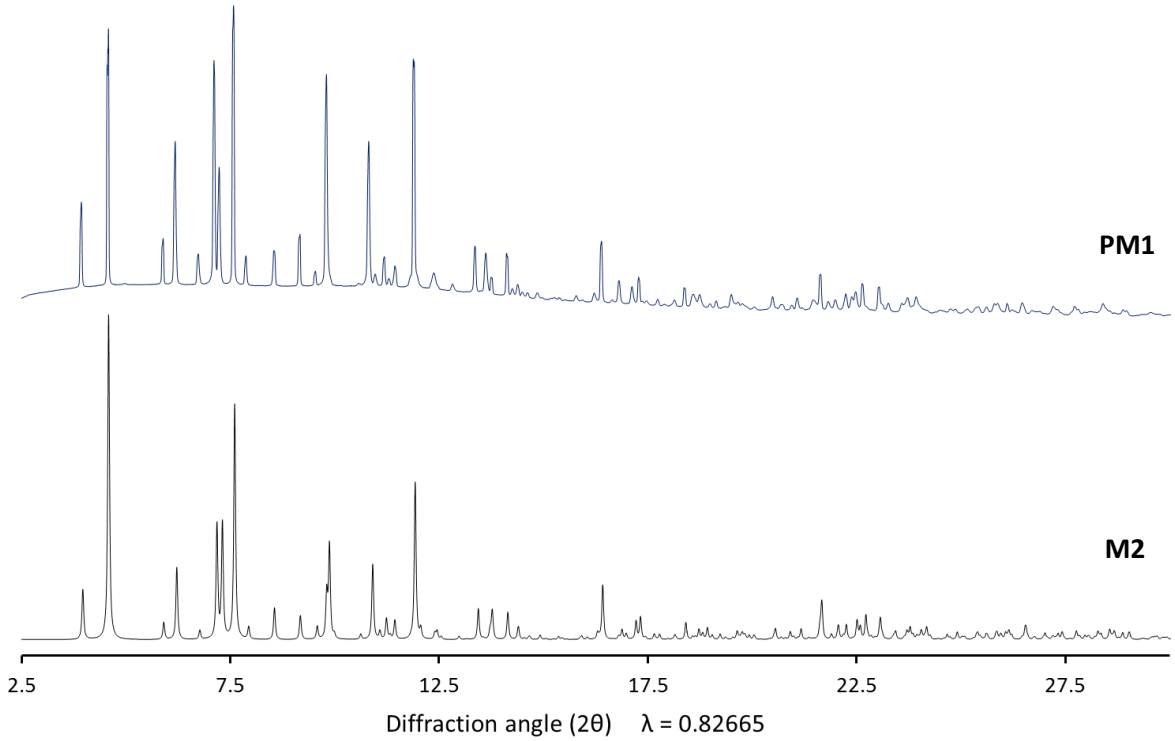

Figure 21 - Powder diffraction pattern of 100% amide-modified MOF $(Me_2NH_2)[In(BDC\text{-}NHC(O)CH_3)_2]$ (**PM1**) (blue) compared to the predicted powder pattern of single crystal structure **M2** (black)

Closer analysis of the powder pattern **PM1** reveals that many of the peaks are split, despite some only corresponding to one set of Miller indices, and being collected on a synchrotron source with a high number of counts. The splitting occurs differently for each reflection therefore is thought to arise from a combination of different closely related phases co-existing within the sample, due to the continuous flexibility of the material, rather than an instrumental problem. Figure 22 shows that the

022 reflection is best represented by 3 different Gaussian curves at different 2θ values (i.e. 3 different phases). This kind of effect was only observed for the parent compound during gas sorption experiments with poor equilibration kinetics. It is suspected that the change in functionality causes stronger interactions with the contained solvent, resulting in poor equilibration of the solvent molecules between different crystallites. The author is unaware of any similar behaviour being reported in the scientific literature, but it would not be expected of typical flexible MOFs showing large defined phase transitions rather than continuously flexible behaviour. Similarly the analysis is only possible due to the precise instrumental set-up at beamline I11,[33, 34] which provides enough data points within one peak to observe the effect of multiple components

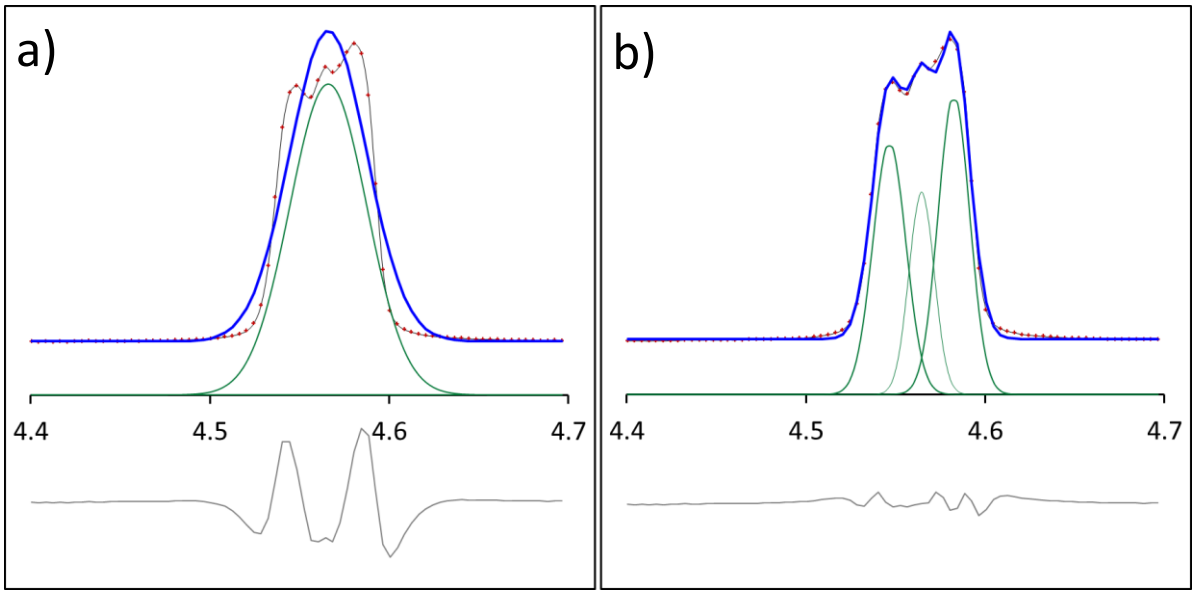

Figure 22 - 022 reflection of powder pattern **PM1** fit with a) 1 Gaussian curve and b) 3 Gaussian curves. Red crosses; experimental points (I_{obs}), blue line; calculated peak (I_{calc}), green line; Gaussian functions responsible for calculated peak, grey; difference map (I_{obs} - I_{calc})

5.4.2 Desolvation studies of methyl amide modified MOF $(Me_2NH_2)[In(BDC\text{-}NHC(O)CH_3)_2$

Unit cell changes

The behaviour the fully modified MOF during solvent removal was explored using *in situ* and *ex situ* heating experiments (**MH1-4**). The details of the experiments can be found in sections 5.3.6 and 5.3.7. The removal of the solvent was seen to result in significant unit cell volume reductions on a similar scale to that observed by the parent compound, but the changes were observed in all 3 crystallographic axes. Examples of the changes are shown in Figure 23, which displays *in situ* heating experiments starting from both a $CHCl_3$- (**MH1**) and a DMF-containing framework (**MH3**).

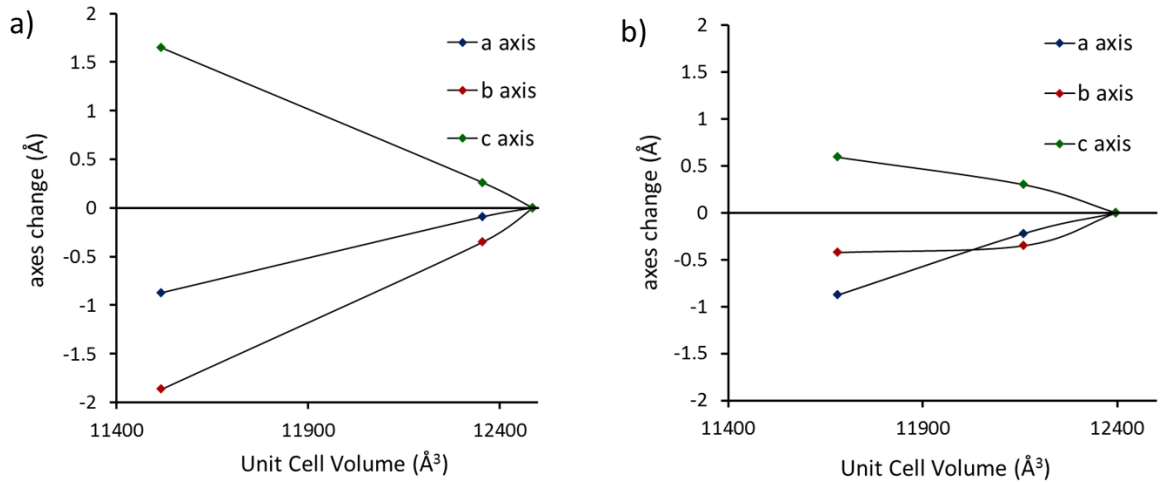

Figure 23 - Changes in the unit cell axes during *in situ* heating experiments of 100% amide-modifed MOF $(Me_2NH_2)[In(BDC\text{-}NHC(O)CH_3)_2]$ containing a) $CHCl_3$ (**MH1**) and b) DMF (**MH3**)

The changes in the *b*- and *c*-axes occur in a similar manner to the breathing trend of the parent compound, with larger changes being observed in the $CHCl_3$-containing framework because it exists in a more open pore form prior to desolvation. The changes in the *a*-axis occur due to a contraction along the helical chains, similar to the initial modification. This effect, unlike in the parent MOF, is highly significant within the flexible behaviour and dominates the change occurring in the DMF containing framework (**MH3**). The breathing therefore is no longer a predominately two-dimensional breathing effect analogous to the wine-rack motions of MIL-53,[43] but has to be considered in all 3

dimensions. In a recent review Jenkins *et al*. comment that breathable motions in 3 dimensions are rare and difficult to achieve within crystalline materials, and have only been seen due to rigid linker twisting or spin crossover effects.[44] One of the few literature examples is MIL-88, which also undergoes a continuous flexibility.[45, 46] Addition of functional groups to the well-studied two-dimensional breathing MOFs, MIL-53 and DMOF, only shows changes the extent of the breathing, not in the type of motion, making the behaviour of $(Me_2NH_2)[In(ABDC)_2]$ quite novel.[10, 47, 48] The change in all axes is allowed due to the diamondoid topology of the MOF, and wouldn't be possible in MIL-53 with its 1D chain of metal ions. The changes in the *a*-axis are illustrated in Figure 24 for *in situ* heating experiments **MH1** and **MH3** ($CHCl_3$- and DMF-containing MOFs respectively) combined with *ex situ* heating study **MH4**. The points are shown in comparison to the single crystal desolvation studies of the parent compound (**1-10**). Trend lines have been drawn to demonstrate the behaviour of the two different solvent systems. The two *in situ* studies can be seen to be converging to the same final point, indicating that unlike the parent MOF, the desolvation results in one thermodynamic minimum for both solvents. Points for **MH2** have not been shown for clarity but agree well with the trend line for the $CHCl_3$-containing MOF.

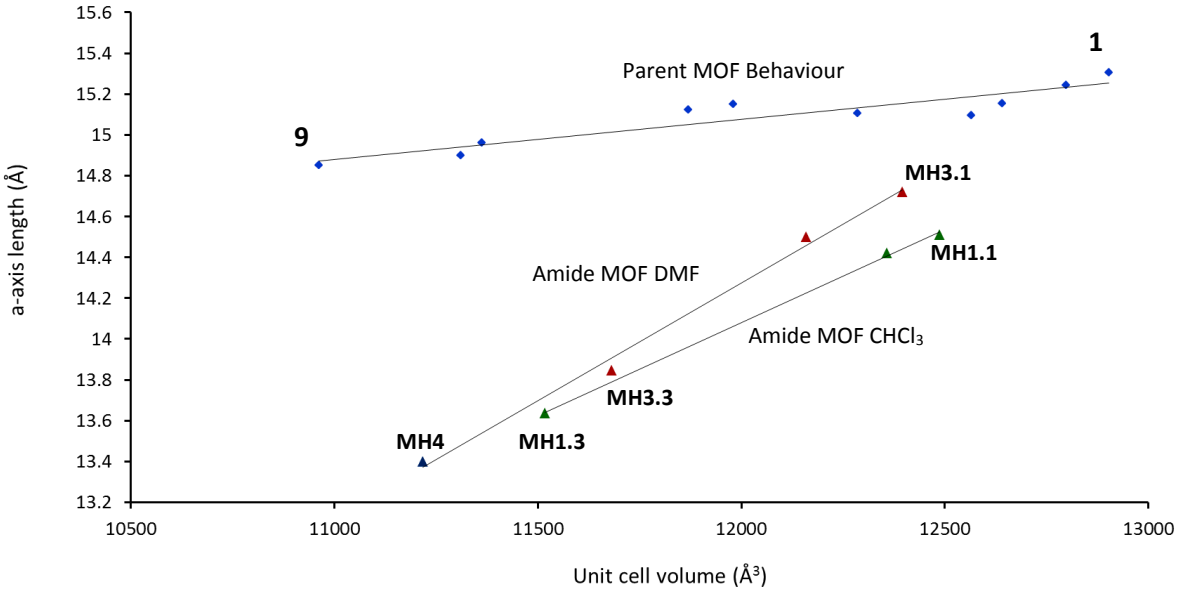

Figure 24 - *a*-axis and unit cell volumes during heating experiments **MH1**, **MH3** and **MH4** on 100% amide-modified MOF $(Me_2NH_2)[In(BDC\text{-}NHC(O)CH_3)_2]$ in comparison to single crystal desolvation studies of as-synthesised $(Me_2NH_2)[In(ABDC)_2]$ (**1-10**)

Structural changes

The full structural solutions of **MH1.3**, **MH3.3** and **MH4** show crystallographic disorder of the amide group over two different sites. This occurs through a rotation of the aromatic ring coupled with a bending out of plane of the amide. The occupancy of the two sites was refined and showed a roughly 50:50 distribution. The asymmetric unit for the framework, showing the disorder, is displayed in Figure 25.

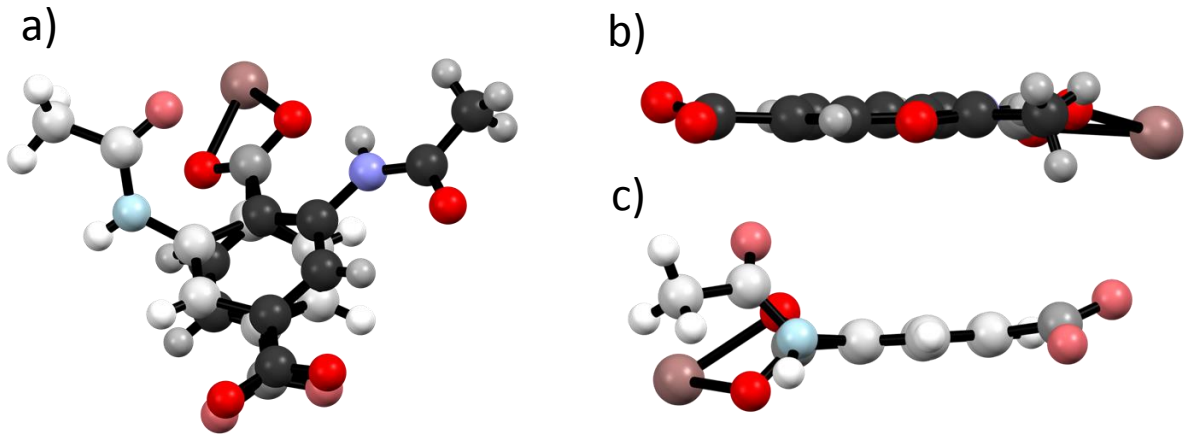

Figure 25 - Ball and stick representation of the asymmetric unit in *ex situ* heated 100% amide-modified MOF $(Me_2NH_2)[In(BDC\text{-}NHC(O)CH_3)_2]$ **MH4**. a) Both parts of the disorder, b) Part 1 of the disorder, c) Part 2 of the disorder. Cations have been removed for clarity···

The disorder of the amide group accompanies the contraction of the helical chains, which causes neighbouring symmetry equivalent amides on the same interpenetrated network to form a very close molecular contact. This is shown in Figure 26 a). In **MH4** the C···C distance of the two methyl groups becomes 2.03 Å (roughly 60% of the sum of van der Waals radii for two carbon atoms) and is too short to exist as an intermolecular interaction. The amide group in the original position therefore can only be 50% occupied and a second position is needed. This position is shown in Figure 26 b). The steric constraints of the neighbouring interpenetrated chain cause the new position to be different to the amine position in the 75%-modified MOF, and the amide group to become bent out of plane, which must involve an energy penalty.

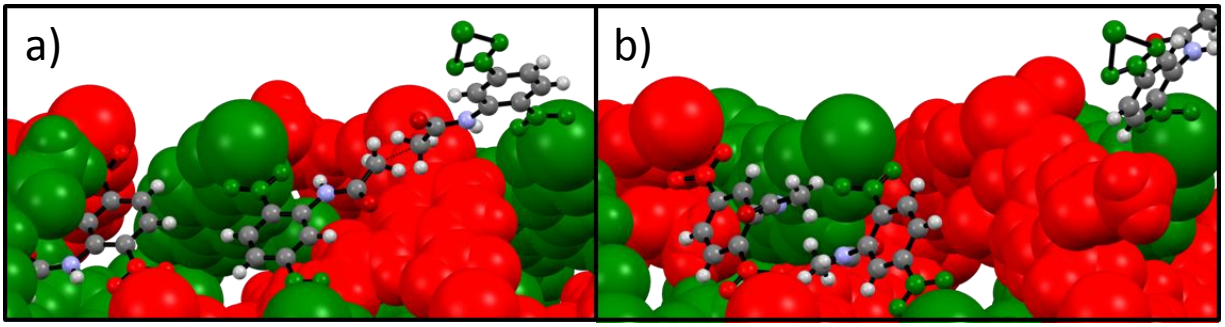

Figure 26 - Ligand environments in *ex situ* heated 100% amide modified MOF $(Me_2NH_2)[In(BDC\text{-}NHC(O)CH_3)_2]$ **MH4** a) Part 1 of the disorder, b) Part 2 of the disorder

The secondary position occurring through a rotation of ligand causes the aromatic ring and the methyl amide to point directly into the channels. This is demonstrated in Figure 27, which compares the pore shape for the two parts of the disorder. The secondary position is only half occupied but is likely to impact significantly on the accessible void volume in the channel.

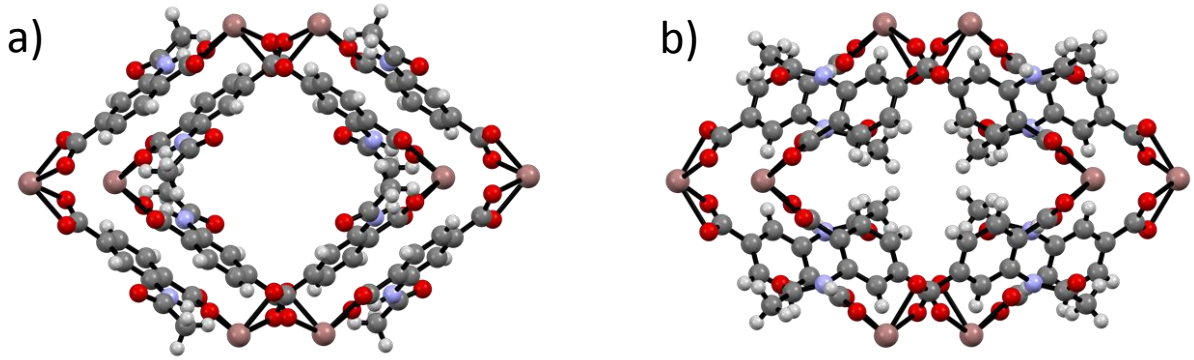

Figure 27 - Ball and stick representation of a single pore in *ex situ* heated 100% amide-modified MOF $(Me_2NH_2)[In(BDC\text{-}NHC(O)CH_3)_2]$ **MH4** . a) part 1 of the disorder, b) part 2 of the disorder. Structure is viewed along the *a*-axis.

5.4.3 CO_2 uptake studies on the methyl amide-modified MOF $(Me_2NH_2)[In(BDC\text{-}NHC(O)CH_3)_2]$

The effect of gas adsorption on the 3D dimensional breathing was studied using *in situ* crystallographic techniques. Full details of the experiments can be found in section 5.3.8. Unfortunately due to time constraints these studies have not yet been benchmarked with corresponding gravimetric adsorption data. The diffraction studies therefore reveal the structural effects of what is believed, but not confirmed, to be incorporation of the gas molecules.

In situ single crystal diffraction study **MI1**

The crystal used for the *in situ* diffraction study (**MI1**) originally contained DMF and was prepared analogously to **MH4**, before mounting in the cell and placing under vacuum. The unit cell of the material showed a reduction along the *a*-axis from the fully solvated version, but only indicative of a partially closed structure. This is thought to arise from difficulties in gas cell preparation during which the sample needs to be exposed to air after heating and can uptake atmospheric water vapour. The *a*-axis and unit cell volume values are shown in Figure 28.

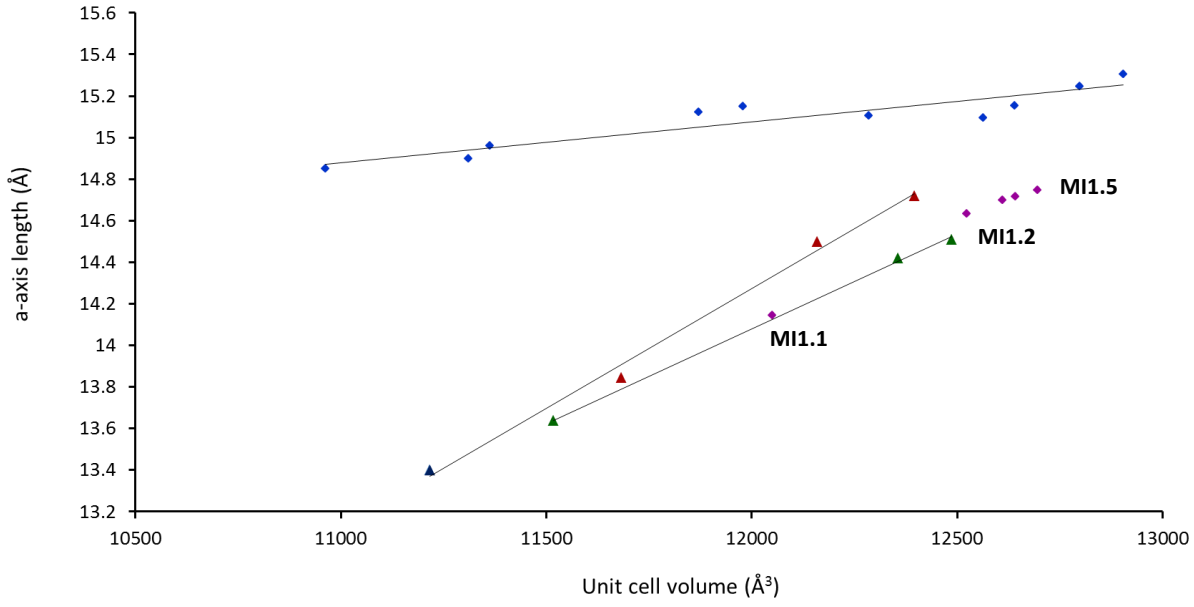

Figure 28 - Data from Figure 24 (see above for details) combined with *in situ* crystallographic study **MI1**

The single crystal X-ray structures obtained after introduction of CO_2 show a movement of the framework back towards structures similar to the fully solvated framework, via an expansion of the helical chains and a pore-opening effect similar to the parent compound. The expansion of the helical chains (*a*-axis) occurred immediately at 1 bar CO_2 (**MI1.2**) but then showed little further increase. In contrast the *b*- and *c*-axes continued to change at higher pressures due to further changes in the pore shape. The changes to all three crystallographic axes are shown in Figure 29 a). Prior to CO_2 loading the framework structure showed the same positional disorder of the amide as previously seen in the desolvation studies. This disorder was removed upon the initial expansion of the helical chains, with part 1 becoming fully occupied. Figure 29 b) plots the C···C distance between methyl groups of the neighbouring amides showing the rapid increase to a value greater than the sum of van der Waals radii. The removal of the amide positional disorder would dramatically increase the channel dimensions, which combined with the removal of the energy penalty for the out of plane amide is thought to drive the process. An analogy can be drawn to gas uptake in ZIF-8, which shows a gate-opening effect involving the swing of the imidazolate linkers during gas sorption.[49, 50] Such dynamic responses, which drastically increase the accessible pore space, have proven beneficial for separations of both gases and molecular mixtures, particularly when the dynamic response occurs for one guest over another.[51–53] After the initial expansion had been achieved the addition of more CO_2 causes the framework to open up the channel in an analogous breathing manner (*b*- and *c*-axis changes) to the parent compound. This is displayed in Figure 30 by plotting the values against the known breathing trend of the parent MOF.

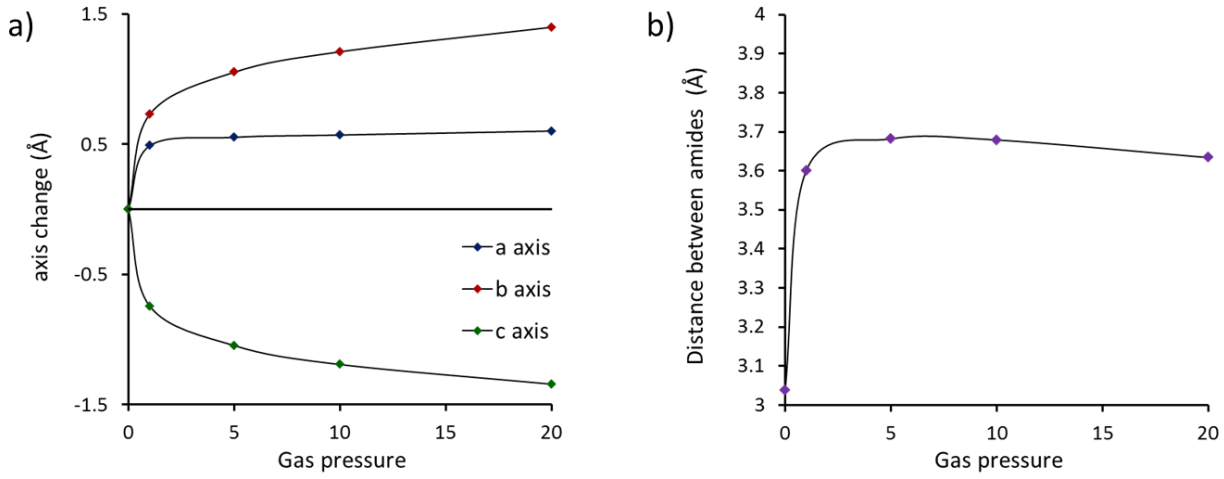

Figure 29 – a) Change in the unit cell parameters and b) change in the C···C distance between methyl groups of neighbouring amides due to increased CO_2 pressure in 100% amide-modified MOF $(Me_2NH_2)[In(BDC\text{-}NHC(O)CH_3)_2]$ during *in situ* crystallographic experiment **MI1**

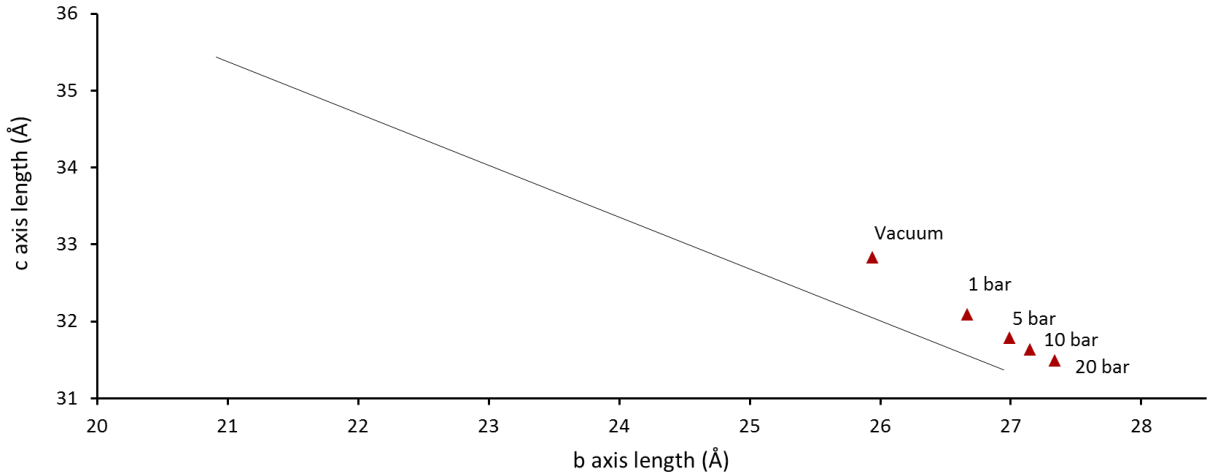

Figure 30 – *b*- and *c*- axis values of 100% amide-modified MOF $(Me_2NH_2)[In(BDC\text{-}NHC(O)CH_3)_2]$ during *in situ* crystallographic CO_2 uptake experiment **MI1** (red triangles). The trendline is based on crystals (**1-10**) of the parent MOF $(Me_2NH_2)[In(ABDC)_2]$ (see chapter 2 for details)

In situ powder diffraction study **MI2**

The desolvation of the $CHCl_3$-containing MOF sample used in **MI2** was carried out using high vacuum only. This was an attempt to reproduce *in situ* study **I7** (chapter 4) to explore if the phase change in the parent MOF to the water-coordinated structure (**C2**) could occur in the modified MOF. The powder pattern under vacuum (**MI2.1**), however, showed no evidence of a new phase and was fitted to the known orthorhombic cell with a single-phase Pawley refinement (Figure 12). The unit cell indicated a fairly open-pore structure with no movement along the *a*-axis, which based on the previous desolvation studies (**MH1-4**), implies minimal levels of desolvation. The $CHCl_3$ solvent is therefore thought to be bound more strongly in the framework, so cannot easily be removed by vacuum, with the amides potentially inhibiting the structural transformation to the water-coordinated phase. Despite this, the CO_2 uptake properties of the mostly solvated structure (**MI2.1**) were still probed (**MI2.2 - MI2.5**). The framework showed a slight opening of the pore indicating that the CO_2 was still being adsorbed and causing dynamic responses for the material. The changes along the trendline of the parent compound are shown in Figure 31

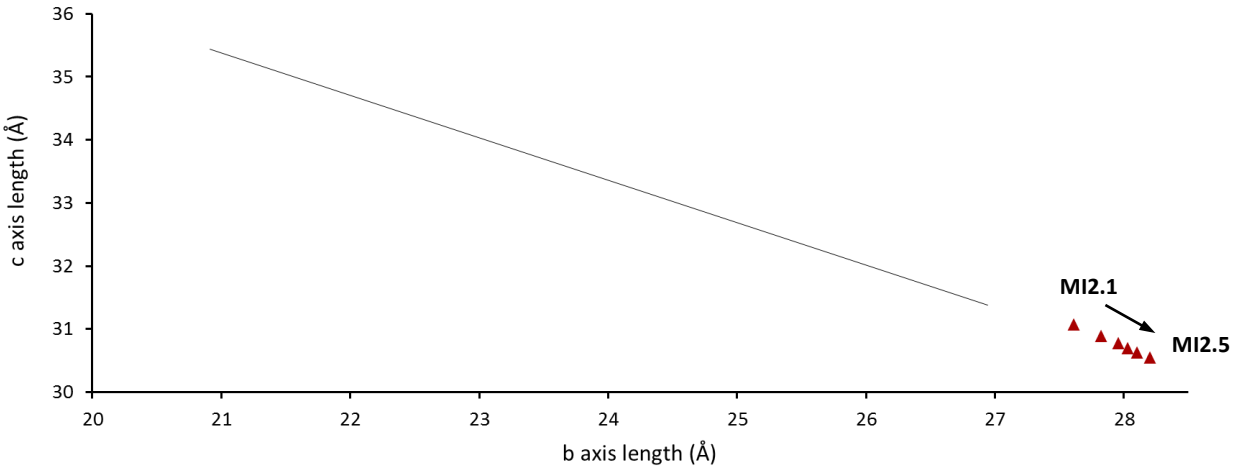

Figure 31 – *b*- and *c*- axis values of 100% amide-modified MOF $(Me_2NH_2)[In(BDC\text{-}NHC(O)CH_3)_2]$ during *in situ* crystallographic CO_2 uptake experiment **MI2** (red triangles). The trend line is based on crystals (**1**-**10**) of the parent MOF $(Me_2NH_2)[In(ABDC)_2]$ (see chapter 2 for details)

Similar to the powder pattern of the fully-solvated MOF, the diffraction peaks of **MI2** associated with certain Miller indices were seen to be split. The splitting of the different peaks was variable across the pressure range recorded and implied a continually changing contribution of different closely related crystalline phases. This suggests that the CO_2 is being adsorbed around the contained $CHCl_3$, causing expansions of the unit cell, but at different rates in different crystallites. A selection of diffraction peaks during the *in situ* is shown in Figure 32.

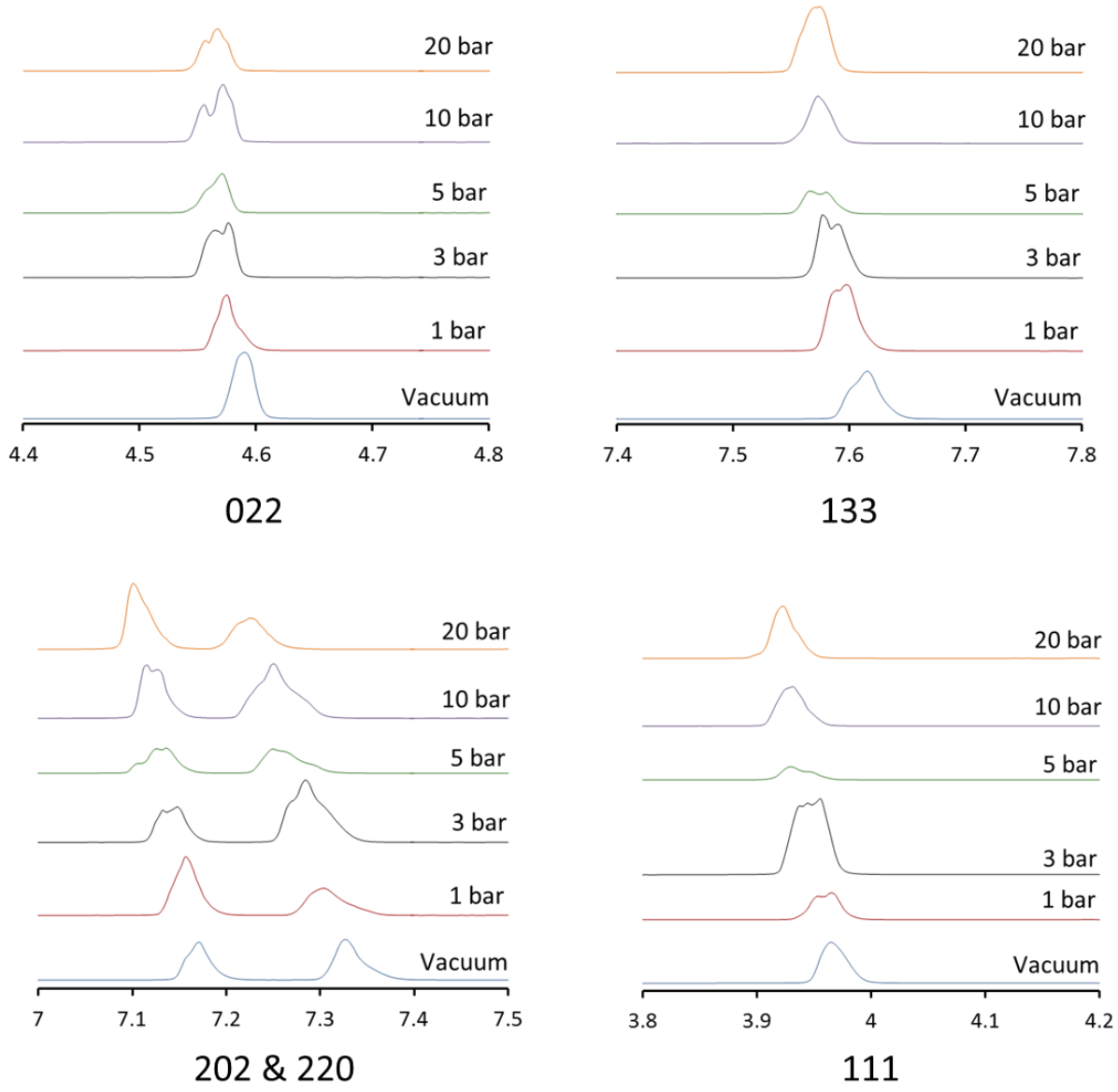

Figure 32 - Selected Miller indices of powder patterned recorded at increasing pressures of CO_2 in in situ diffraction study **MI2**

5.4.4 Post-synthetic modification of the amino group in $(Me_2NH_2)[In(ABDC)_2]$ using maleic anhydride

The modification of the amine group was also demonstrated using a ring opening reaction on maleic anhydride. This reaction was previously reported on UiO-66 in a 25% conversion.[19]

Post-synthetic modification of the amino group using maleic anhydride, see section 5.3.2, used the same synthetic conditions as the acetamide modification and also occurred in a single crystal manner. Unfortunately a lower conversion than for the amide was achieved, but residual electron density peaks corresponding to the added functionality could clearly been seen when modelling the crystal structure. The rigid structure formed due to the presence of the double bond allowed the new functionality to be successfully modelled crystallographically at a 25% occupancy using restraints (**M4**). This correlates well the previous work on UiO-66, using similar conditions.[19] The displacement parameters of the modified group increased on moving further along the chain from the point of attachment, most likely due to some movement of the group, but could not be fully modelled due to the small amount of electron density it accounted for. The increased length of the modified group compared to the amide also caused the refinement to be complicated due to overlap of symmetry equivalent groups on a neighbouring ligand. This is displayed in Figure 33. Further investigation is required but the increased size of the group would most likely inhibit the conversion above 50% without substantial expansion of the helical chains.

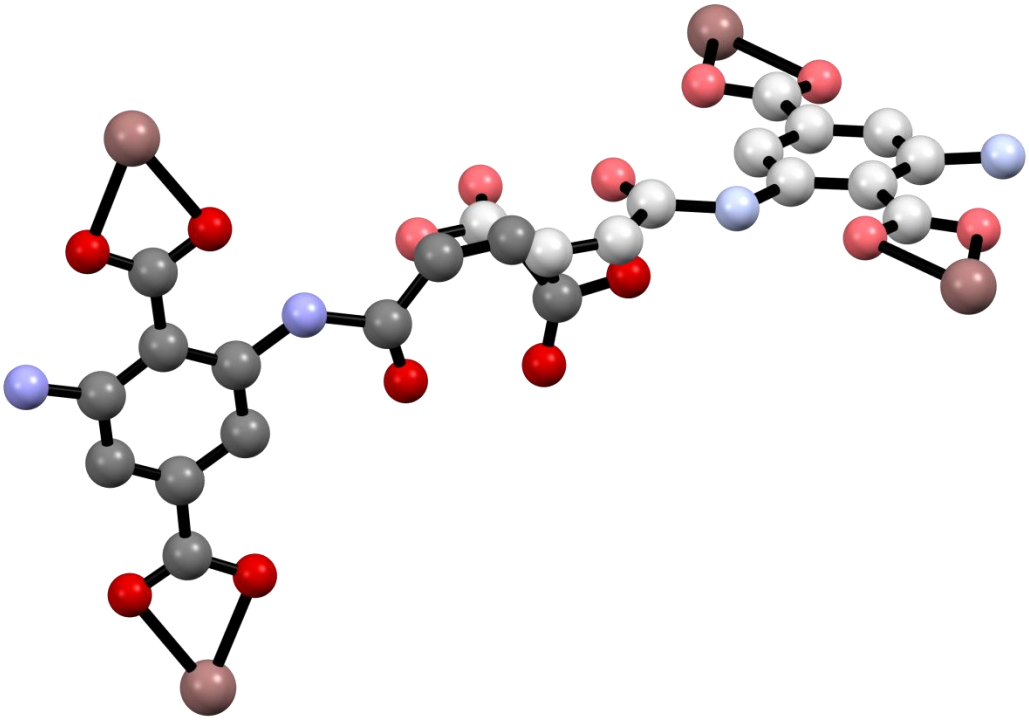

Figure 33 - Ball and stick representation of two neighbouring ligands, in which the 25% maleic anhydride-modified MOF $(Me_2NH_2)[In(ABDC)_{1.5}(BDC\text{-}NHC(O)CHCHC(O)OH)_{0.5}]$ (**M4**) results in direct overlap of the new functional groups. Hydrogens have been removed for clarity

Similar to the amide modification, the addition of the new framework atoms occurs predominantly along the *a*-axis, resulting in the framework still exhibiting 1 dimensional channels containing the cation and solvent molecules. The framework exhibits a solvent accessible void about 85% the size of the 100% amide-modified MOF (**M2**). The bulk sample was analysed using X-ray powder diffraction (**PM4**) and showed a reasonably good match to the predicted pattern from the refined single crystal structure **M4** (Figure 34). There is also evidence of a small quantity the water-coordinated phase of the parent MOF present in the pattern, but because the MOF isn't fully modified, it is unknown if the crystallites showing the water-coordinated phase have also undergone PSM.

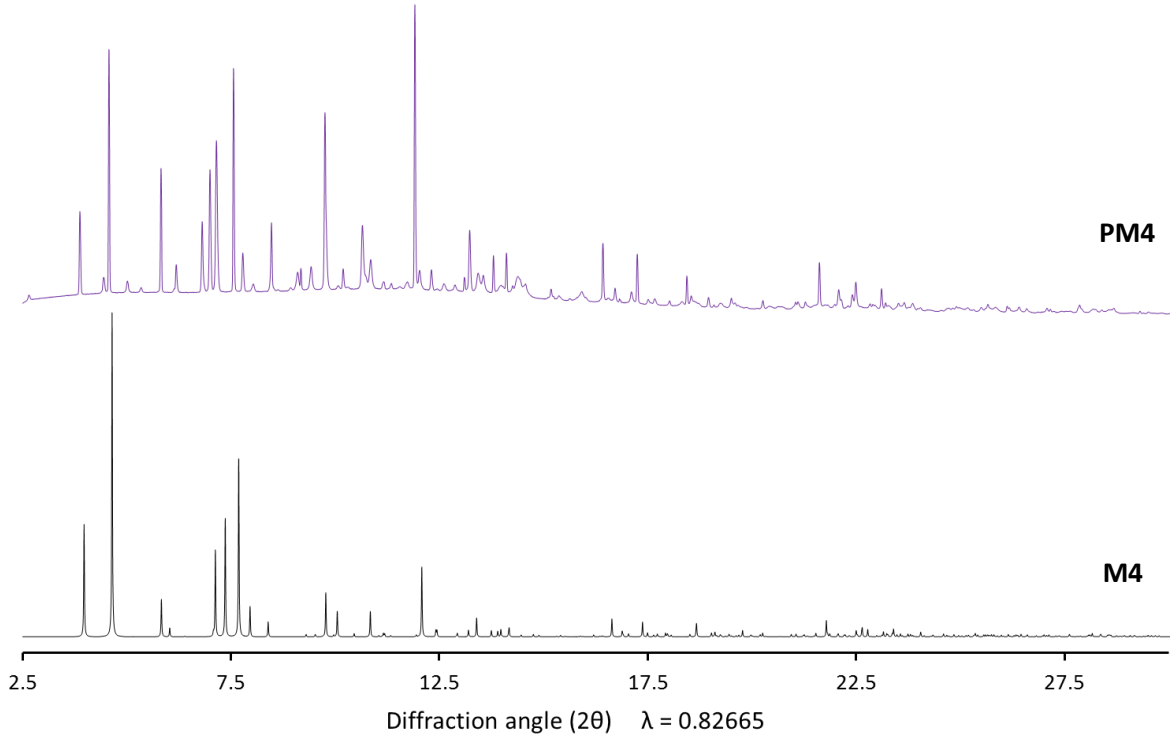

Figure 34 - PXRD pattern of 25% maleic anhydride-modified MOF $(Me_2NH_2)[In(ABDC)_{1.5}(BDC\text{-}NHC(O)CHCHC(O)OH)_{0.5}]$ **PM3** (purple) compared to the predicted pattern from corresponding single crystal diffraction experiment **M4** (black)

The modified structure shows very similar unit cell changes to that shown by the 75% amide-modified MOF, displaying an open structure along the *b*- and *c*-axis trend line of the parent compound, but a shortening of the *a*-axis resulting in a decreased unit cell volume. These effects are shown in Figure 35 and Figure 36 in comparison to the 75% amide-modified MOF study **M1**. This effect implies that even minor conversions, resulting in a slight removal of the amine-amine contact of the parent MOF, are enough to drive the contraction of the helical chains. The desolvation for the framework has not yet been studied, but is expected to be similar to that of the amide-modified version.

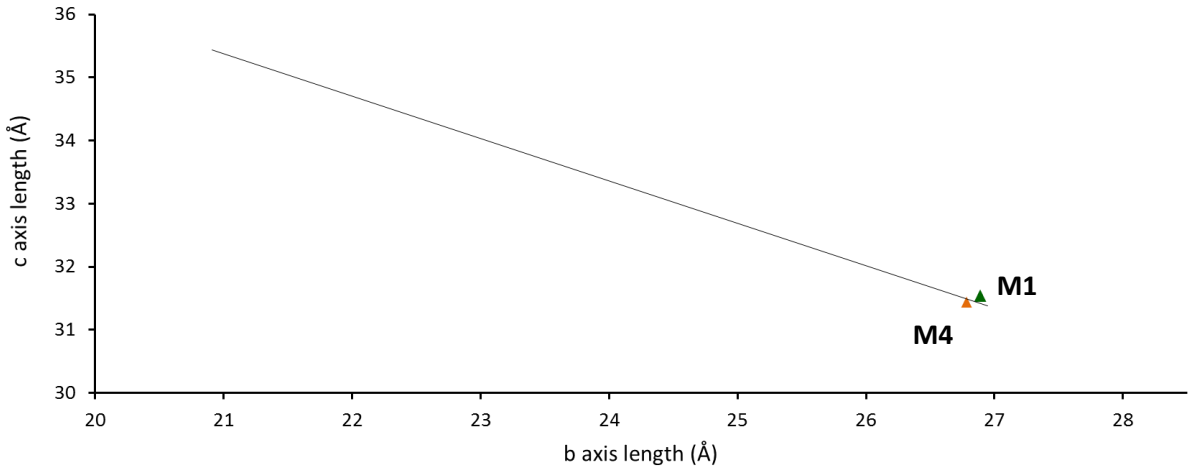

Figure 35 – *b*- and *c*-axis lengths obtained for 25% maleic anhydride-modified MOF $(Me_2NH_2)[In(ABDC)_{1.5}(BDC\text{-}NHC(O)CHCHC(O)OH)_{0.5}]$ (**M4**) (orange triangle) in comparison to 75% amide modified MOF $(Me_2NH_2)[In(BDC\text{-}NHC(O)CH_3)_{1.5}(ABDC)_{0.5}]$ (**M1**) (green triangle). The trend line is based on single crystal desolvation studies of as-synthesised parent MOF ($(Me_2NH_2)[In(ABDC)_2]$) (**1-10**) (see chapter 2 for details)

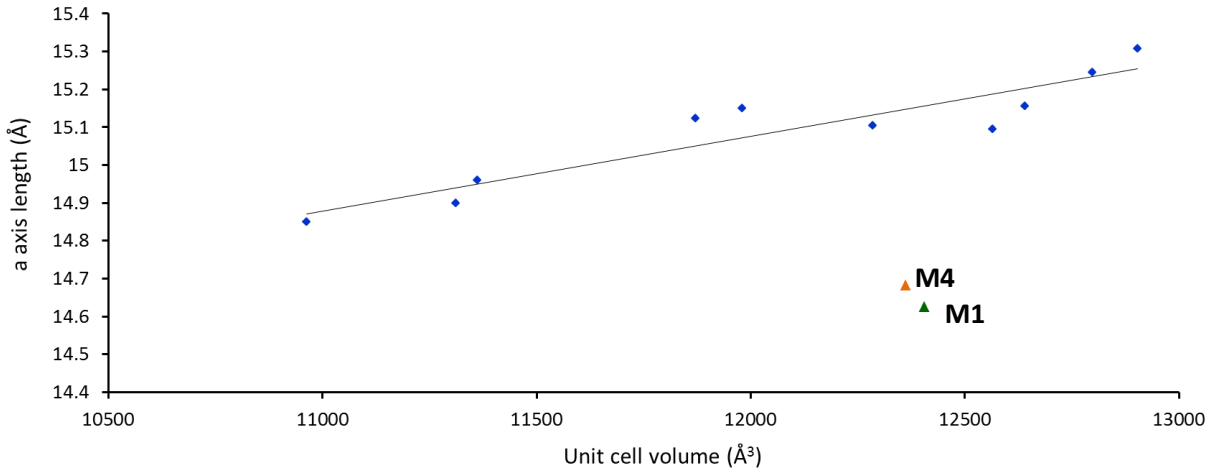

Figure 36 – *a*-axis and unit cell volumes obtained for 25% maleic anhydride-modified MOF $(Me_2NH_2)[In(ABDC)_{1.5}(BDC\text{-}NHC(O)CHCHC(O)OH)_{0.5}]$ (**M4**) (orange triangle) in comparison to 75% amide modified MOF $(Me_2NH_2)[In(BDC\text{-}NHC(O)CH_3)_{1.5}(ABDC)_{0.5}]$ (**M1**) (green triangle) and single crystal desolvation studies of as-synthesised parent MOF ($(Me_2NH_2)[In(ABDC)_2]$) (**1-10**) (see chapter 2 for details)

5.4.5 Post-synthetic cation exchange in $(Me_2NH_2)[In(ABDC)_2]$ using Ag^+ ions

Cation exchange was attempted using several different methods (A-C), which are detailed in section 5.3.2. All the conversions occurred in a single crystal - single crystal manner and full single crystal X-ray diffraction data sets were obtained (**S1-5**). Refinements of the structures showed reasonably well-defined positions for the new Ag^+ ion, with the electron density located near the amino group. The distance between the Ag^+ and nitrogen ranged from 2.2-2.3Å. Figure 37 shows a histogram of all silver nitrogen distances in the Cambridge Structural Database (CSD), and suggests that this is typical for a silver nitrogen bond.

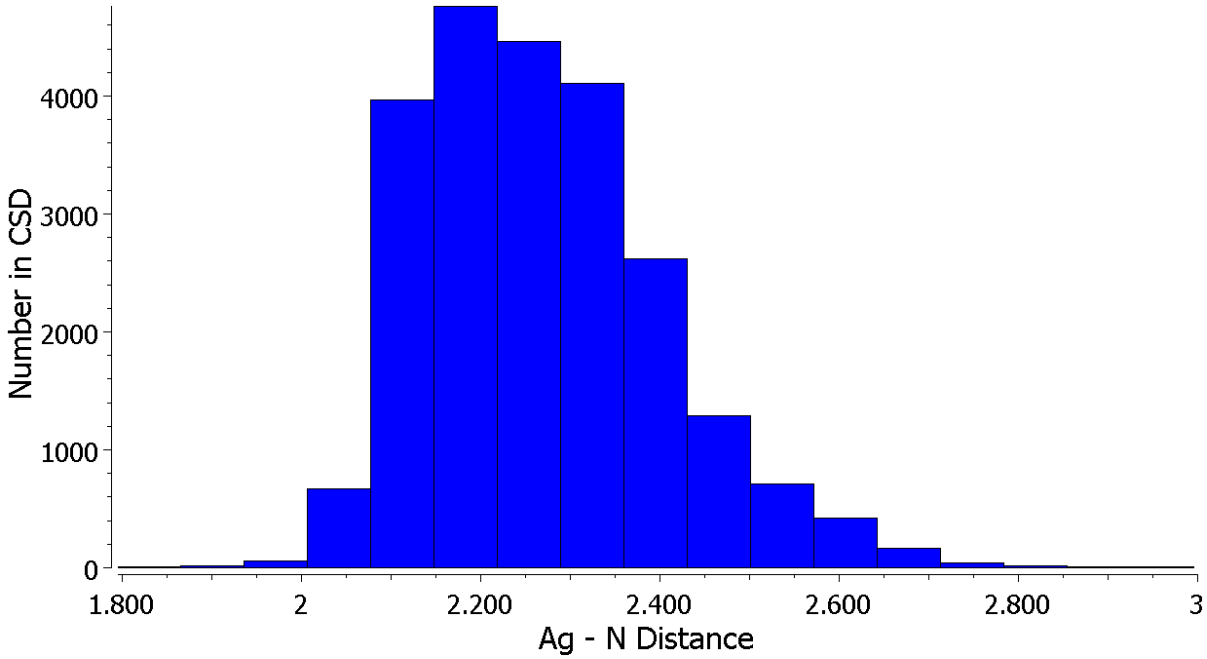

Figure 37 - Histogram created from structures deposited in the CSD containing Ag-N bonds. The data was plotted using Mercury[54]

The Ag^+ ion was able to be modelled anisotropically in all of the structures, at refined occupancies ranging between 24 – 33%. The asymmetric unit contains half an indium centre and therefore half a cation, so these occupancies correspond to a cation exchange of 48-66%. Although these models showed stable least-squares refinements, large electron density peaks of magnitude 3 – 5 e^- / $Å^3$, were located close to the Ag^+ ion in several of the structures (**S2** and **S3**). These electron density peaks were too close to be bound solvent molecules, and implied a slight disorder of the Ag^+ ion. Splitting the Ag^+ ion into 4 parts, each modelled isotropically allowed the model to account for the

surrounding electron density and increased the overall occupancy in the structures to values between 35 – 40% (70 to 80% conversion). The two different methods for modelling the asymmetric unit in **S3** are shown in Figure 38. All three synthetic conditions (A-C) showed fairly similar conversions and so far no suitable bulk analysis for accurately quantifying the overall conversion percentage has been carried out. The best conversion method is therefore unknown, but in general all three methods can be estimated to be between 50 – 80%, most likely varying crystallite to crystallite.

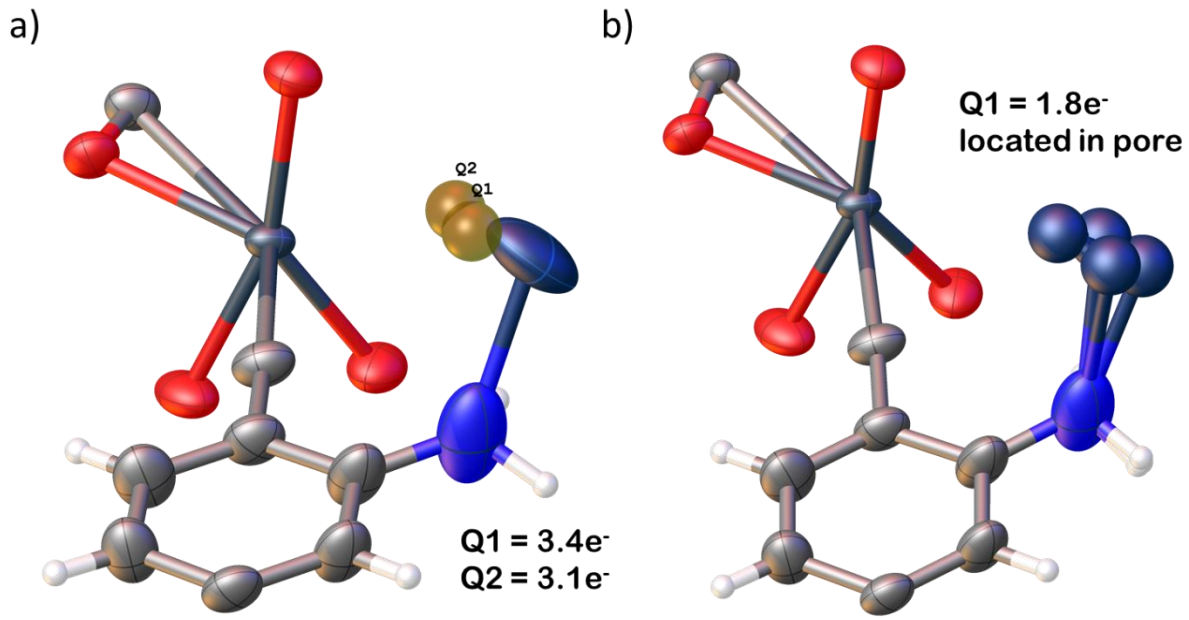

Figure 38 - Asymmetric unit of Ag^+ ion-exchanged MOF $(Me_2NH_2)_{(1-x)}Ag_x[In(ABDC)_2]$ (**S3**) modelled with a) one location of the Ag^+ ion, modelled anisotropically, and b) 4 disordered locations of the Ag^+ ion, modelled isotropically. Carbon atoms are in grey, oxygen atoms in red, nitrogen atoms in blue, hydrgeon atoms in white, indium atoms in grey, silver atoms in dark blue and residudual peaks of electron denisty (Q peaks) in brown.

The cation exchange occurs while maintaining the same amine position as the parent MOF, and therefore the same amine-amine hydrogen bonding interaction to the neighbouring interpenetrated chain. This can occur because unlike the PSM the connected Ag^+ ion sits above or below the aromatic rings rather than in the plane of the ring. This is shown in Figure 39 a) and results in the Ag^+ ion pointing directly into the accessible pore space Figure 39 b).

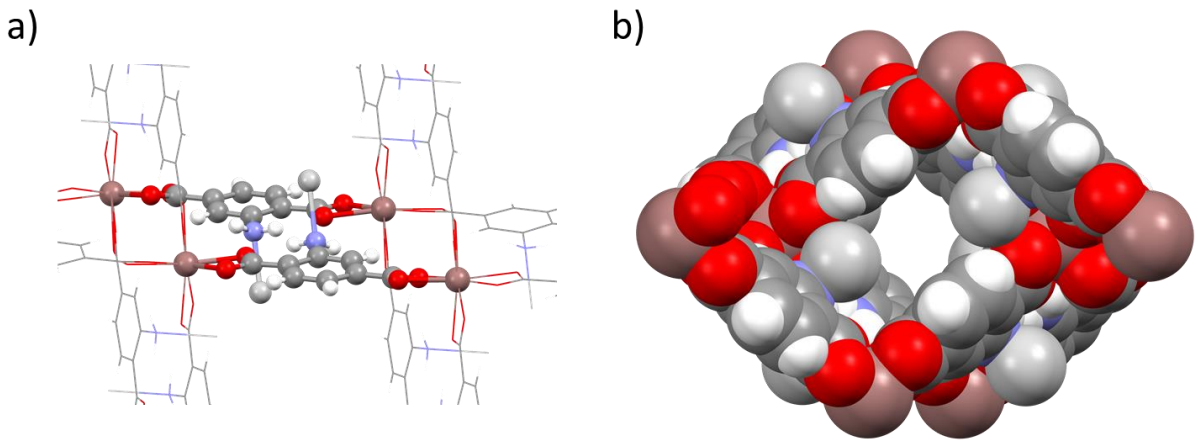

Figure 39 - a) Location of Ag^+ ions in Ag^+ ion-exchanged MOF $(Me_2NH_2)_{(1-x)}Ag_x[In(ABDC)_2]$ (**S5**) showing the maintenance of the amine-amine interaction seen in the parent MOF $(Me_2NH_2)[In(ABDC)_2]$ (**1**). b) Ag^+ ion-exchanged MOF $(Me_2NH_2)_{(1-x)}Ag_x[In(ABDC)_2]$ (**S5**) showing the partial occupancy Ag^+ ions pointing into the channel.

The Ag^+ ion shows an interaction with the carboxyl oxygen on the neighbouring interpenetrated chain (roughly 89% of the sum of van der Waals radii for the two atoms) but is also likely coordinated to guest solvent molecules. If the solvent could be removed it would provide a potential open metal site for improving the guest uptake properties. Studies on MOFs containing open metal sites (CPO-27,[55–59] HKUST-1,[56, 60–63] and $[Mn(DMF)_6]_3[(Mn_4Cl)_3(BTT)_8(H_2O)_{12}]_2$)[64, 65] (BTT = 1,3,5-benzenetristetrazolate) have shown that they dominate the gas binding locations, often with interactions at distances shorter than the sum of van der Waals radii. Studies on MIL-101[2] and $H_3[(Cu_4Cl)_3(BTTri)_8]$[3] (BTTri = 1,4-benzenedi(1*H*-1,2,3-triazole)) have also shown the potential for binding of organic amines to open metal sites. Even without removing the solvent, molecules introduced into the pore might still be able to strongly interact with the Ag^+ ions, due to the ability of Ag(I) to exist in a wide variety of coordination environments. This may improve guest retention or allow Ag^+ ion-based catalytic processes.

The purity of the bulk sample was checked through X-ray powder diffraction (**PS1**), it was able to be successfully fitted to single phase using Pawley refinements and showed reasonably good match to the predicted pattern from the single crystal structure (**S5**). A comparison of the predicted and experimental patterns can be seen in Figure 40.

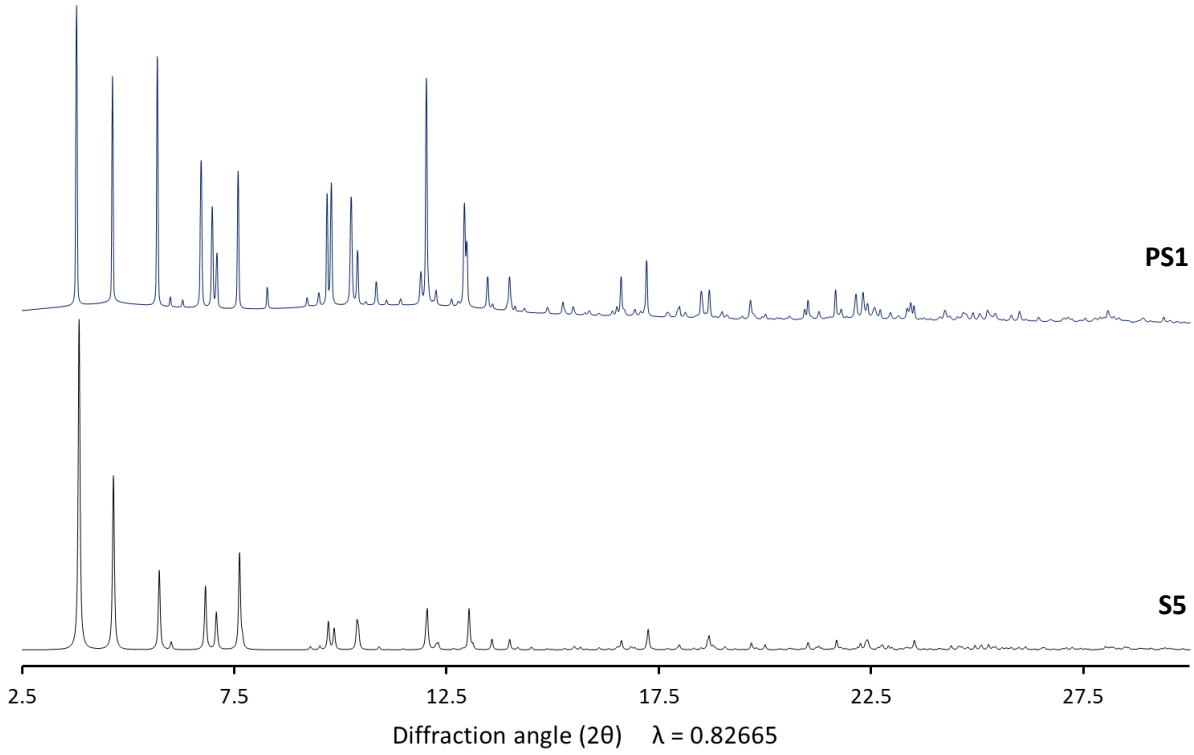

Figure 40 – Experimental PXRD pattern of Ag^+ ion exchanged MOF $(Me_2NH_2)_{(1-x)}Ag_x[In(ABDC)_2]$ (**PS1**) (blue) compared to the predicted pattern from corresponding single crystal structure **S5** (black)

The *b*- and *c*-axes lengths of the Ag^+ ion exchanged MOF corresponded reasonably well to the parent MOF and showed an open-pore structure along the known breathing trend line, although the frameworks showed an increase in the *a*-axis length. This is the opposite behaviour of the amide-modified framework, and is thought to originate from the amine-amine interaction still occurring but with the added presence of the coordinated Ag^+ ion.

The breathing effect on solvent removal was attempted to be studied analogously to the parent MOF, but unfortunately extended heating of the modified framework resulted in a loss in the crystallinity, most likely due to the relatively weak coordination of the Ag^+ ion, which is only bound through one nitrogen atom. Similarly the MOF containing the Ag^+ ion was incredibly light sensitive and had to be kept in the dark. While this made solvent removal studies very difficult, a weak data set of a partially desolvated single crystal structure was obtained by only heating a crystal at 100°C in the absence of any light (**SH1**).

The desolvation seemed to occur through changes in all three axis dimensions. The changes in the *b*- and *c*-axes are shown in Figure 41 and can be seen to correlate well to the known breathing trend of the parent MOF (**1-10**). The changes in the a-axis, shown in Figure 42, follow a similar trend to the DMF containing amide (**MH3-4**).

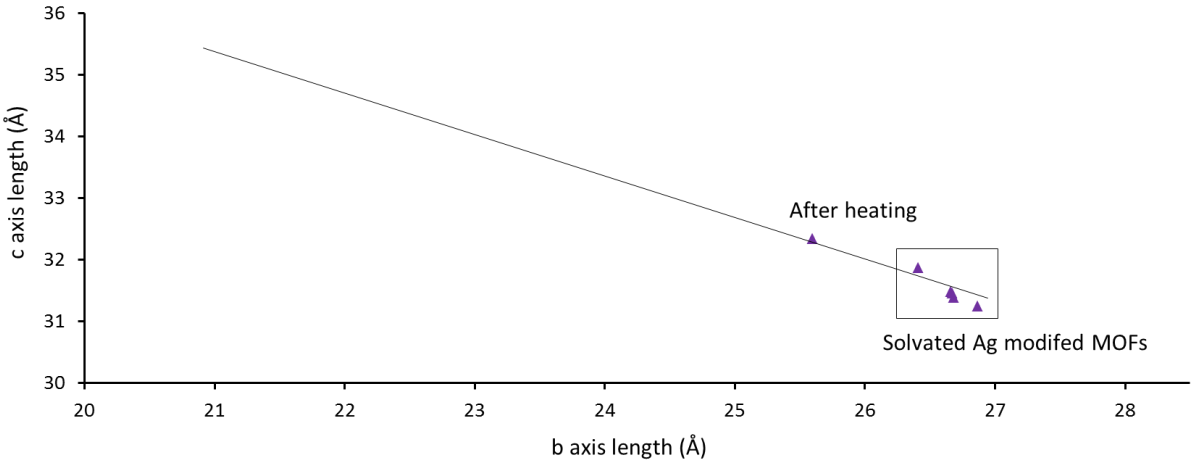

Figure 41 – *b*- and *c*-axis values obtained for solvated Ag^+ ion-exchanged MOF $(Me_2NH_2)_{(1-x)}Ag_x[In(ABDC)_2]$ (**S1-5**) and heated MOF (**SH1**). The trend line is based on single crystal desolvation studies of as-synthesised parent MOF ($(Me_2NH_2)[In(ABDC)_2]$) (**1-10**) (see chapter 2 for details)

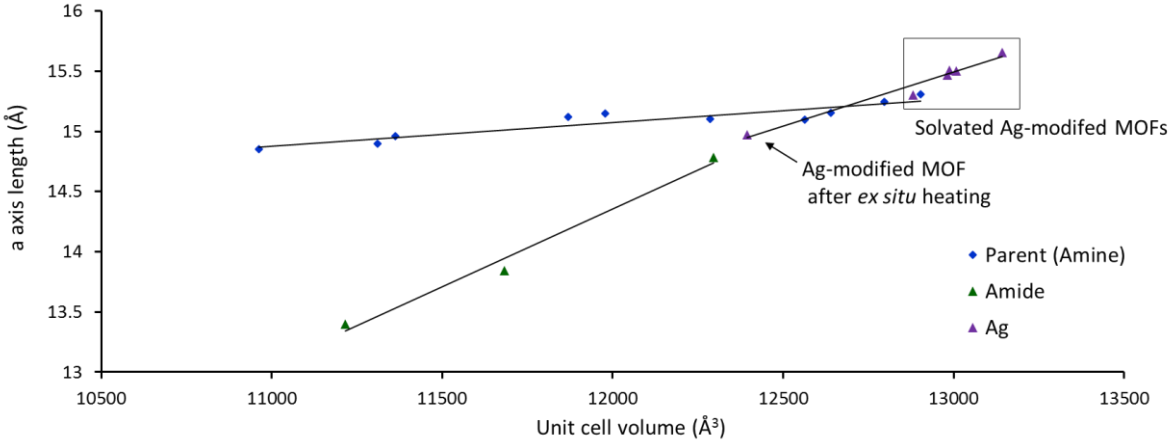

Figure 42 – *a*-axis and unit cell volumes obtained for solvated Ag^+ ion-exchanged MOF $(Me_2NH_2)_{(1-x)}Ag_x[In(ABDC)_2]$ (**S1-5**) and heated MOF (**SH1**) (blue diamonds), DMF-exchanged 100% amide modified MOF $(Me_2NH_2)[In(BDC\text{-}NHC(O)CH_3)_2]$ (green triangles) and of as-synthesised parent MOF $(Me_2NH_2)[In(ABDC)_2]$ (**1-10**).

The partially desolvated crystal structure **SH1** displays a clear disorder of the nitrogen position. This occurs because the contraction of the helical chains changes the distance between two neighbouring ligands and it becomes favourable to disorder the nitrogen position to form a second interaction with the Ag^+. This could occur to all the Ag^+ ions, because the stoichiometry only allows for one cation per two dicarboxylate ligands. The disorder and interactions are displayed in Figure 43.

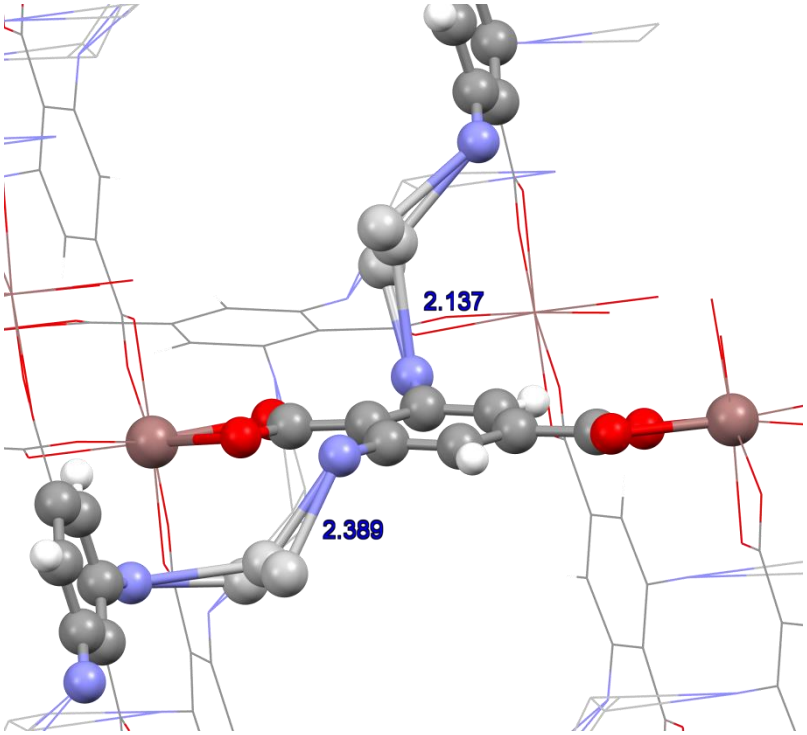

Figure 43 - Ball and stick representation of partially desolvated Ag^+ ion-exchanged MOF $(Me_2NH_2)_{(1-x)}Ag_x[In(ABDC)_2]$ (**SH1**), displaying interactions of Ag^+ with two disordered amine positions

5.5 Conclusions

The modification of $(Me_2NH_2)[In(ABDC)_2]$ has been fairly easily achieved while maintaining the single crystal crystallinity of the material. This has allowed for confirmation of the modifications and in-depth analysis of the structural rearrangements that occur. The conversion to the methyl amide has been demonstrated at quantitative conversion and the breathing effect explored. Although further studies on the amide are needed to understand the limit of the flexibility, it is clear that it occurs on a similar scale to the parent MOF but in a 3-dimensional manner rather than the predominantly 2-dimensional breathing of the parent amine MOF. The framework structure differs between the fully solvated DMF- and $CHCl_3$-containing frameworks, implying a solvent dependence, but the desolvation now appears to result in the same solvent-free structure. This desolvated structure involves a disorder of the amide position occurring via a linker rotation that blocks the accessible channel. The effects of the amide modification are therefore significantly different to the incorporation of functional groups in other flexible MOFs which tend to only affect the extent of the frameworks intrinsic breathing mode.

In situ CO_2 studies of a partially desolvated framework shows that the flexibility is reversible on gas uptake and follows the trend observed during desolvation. The same behaviour is expected for a fully desolvated system but has not yet been studied. The structural changes have also not yet been able to be compared to appropriate gravimetric studies, which would be the next step for further study. The structural effects shown so far appear to be continuous, but more data points are required.

The amide appears to be more stable within $CHCl_3$, air and vacuum, not showing any evidence of conversion to the water-bound phase seen for the parent MOF. This could be due to a stronger binding of solvent or water to the new functional group, or lack of space for the necessary rearrangement to the octahedral geometry at the indium centres due to the increased size of the ligand.

PSM has also been demonstrated for larger functional groups via a ring opening reaction, and suggests that the MOF is suitable for a wide variety of different modifications. These present both a method for adding new functionality into the framework and adjusting the breathing behaviour. These types of studies have previously been presented in the literature for the narrow-pore to large-pore breathing mode of DMOF, where the gate pressure during gas sorption has been altered with various ether based side groups,[10] but $(Me_2NH_2)[In(ABDC)_2]$ offers the chance to potentially design a specific size or specific dimensionality of breathing effect by choosing the right set of chemical modifications to the framework.

Cation exchange using Ag^+ ions has also been demonstrated in a SC-SC process and initial results suggest it also affects the flexibility of the material. The Ag^+ ions were able to be crystallographically modelled within the pore of the framework after the exchange, and can be seen to be directly bound to the free amine. Accurately quantifying the conversion of the bulk sample however has not yet been achieved and will require exploration of alternative methods. One possibility would be ICP-MS which should be able to obtain a ratio between the silver and indium. The presence of the Ag^+ ion pointing into the pore space also presents an open metal site and suggests potential applications in catalysis or gas separations.

The role the cation plays in the flexibility is currently largely unknown, but it is hoped further studies with other cations combined with accurate characterisation of the flexibility, would help probe its involvement. A wide range of different cations could be chosen to replace the dimethyl ammonium ion, assuming they fit inside the pore. These include a variety of similar organic ions or a series of mono charged inorganic ions. The organic cations could range in size from ammonium to tetrabutyl ammonium, or contain added functionality such as choline $(CH_3)_3N^+CH_2CH_2OH$. Organic cations such as these could be more readily characterised using solution phase ^1H NMR of the digested material.

5.6 References

1 B. Arstad, H. Fjellvåg, K. O. Kongshaug, O. Swang, and R. Blom, *Adsorption*, 2008, 14, 755–762.

2 Y. K. Hwang, D.-Y. Hong, J.-S. Chang, S. H. Jhung, Y.-K. Seo, J. Kim, A. Vimont, M. Daturi, C. Serre, and G. Férey, *Angew. Chem. Int. Ed.*, 2008, 47, 4144–4148.

3 A. Demessence, D. M. D'Alessandro, M. L. Foo, and J. R. Long, *J. Am. Chem. Soc.*, 2009, 131, 8784–8786.

4 R. Vaidhyanathan, S. S. Iremonger, K. W. Dawson, and G. K. H. Shimizu, *Chem. Commun.*, 2009, 5230–5232.

5 R. Vaidhyanathan, S. S. Iremonger, G. K. H. Shimizu, P. G. Boyd, S. Alavi, and T. K. Woo, *Science*, 2010, 330, 650–653.

6 J.-B. Lin, W. Xue, J.-P. Zhang, and X.-M. Chen, *Chem. Commun.*, 2011, 47, 926–928.

7 P.-Q. Liao, D.-D. Zhou, A.-X. Zhu, L. Jiang, R.-B. Lin, J.-P. Zhang, and X.-M. Chen, *J. Am. Chem. Soc.*, 2012, 134, 17380–17383.

8 S. Yang, J. Sun, A. J. Ramirez-Cuesta, S. K. Callear, W. I. F. David, D. P. Anderson, R. Newby, A. J. Blake, J. E. Parker, C. C. Tang, and M. Schröder, *Nat. Chem.*, 2012, 4, 887–894.

9 T. Devic, F. Salles, S. Bourrelly, B. Moulin, G. Maurin, P. Horcajada, C. Serre, A. Vimont, J.-C. Lavalley, H. Leclerc, G. Clet, M. Daturi, P. L. Llewellyn, Y. Filinchuk, and G. Férey, *J. Mater. Chem.*, 2012, 22, 10266-10273.

10 S. Henke, A. Schneemann, A. Wütscher, and R. a Fischer, *J. Am. Chem. Soc.*, 2012, 134, 9464–9474.

11 S. M. Cohen, *Chem. Rev.*, 2012, 112, 970–1000.

12 Y. Tan, Y. Zhang, Y. He, Y. Zheng, and J. Zhang, *Inorg. Chem.*, 2014, 53, 12973–12976.

13 M. Kim, J. F. Cahill, H. Fei, K. a Prather, and S. M. Cohen, *J. Am. Chem. Soc.*, 2012, 134, 18082–18088.

14 Z. Wang and S. M. Cohen, *J. Am. Chem. Soc.*, 2009, 131, 16675–16677.

15 M. Servalli, M. Ranocchiari, and J. A Van Bokhoven, *Chem. Commun.*, 2012, 48, 1904–1906.

16 Z. Wang and S. M. Cohen, *J. Am. Chem. Soc.*, 2007, 129, 12368–12369.

17 S. J. Garibay, Z. Wang, and S. M. Cohen, *Inorg. Chem.*, 2010, 49, 8086–8091.

18 M. Kandiah, S. Usseglio, S. Svelle, U. Olsbye, K. P. Lillerud, and M. Tilset, *J. Mater. Chem.*, 2010, 20, 9848-9851.

19 S. J. Garibay and S. M. Cohen, *Chem. Commun.*, 2010, 46, 7700–7702.

20 T. Ahnfeldt, D. Gunzelmann, J. Wack, J. Senker, and N. Stock, *CrystEngComm*, 2012, 14, 4126-4136.

21 M. Huang, G. Chang, Y. Su, H. Xing, Z. Zhang, Y. Yang, Q. Ren, Z. Bao, and B. Chen, *Chem. Commun.*, 2015, 51, 12205–12207.

22 G. Chang, M. Huang, Y. Su, H. Xing, B. Su, Z. Zhang, Q. Yang, Y. Yang, Q. Ren, Z. Bao, and B. Chen, *Chem. Commun.*, 2015, 51, 2859–2862.

23 A. B. Pangborn, M. a. Giardello, R. H. Grubbs, R. K. Rosen, and F. J. Timmers, *Organometallics*, 1996, 15, 1518–1520.

24 SMART APEX II, *Bruker AXS, Madison, Wisconsin, USA*.

25 R. H. Blessing, *Acta Crystallogr. A* ., 1995, 51, 33–38.

26 L. Krause, R. Herbst-Irmer, G. M. Sheldrick, and D. Stalke, *J. Appl. Cryst.*, 2015, 48, 3–10.

27 H. Nowell, S. a. Barnett, K. E. Christensen, S. J. Teat, and D. R. Allan, *J. Synchrotron Radiat.*, 2012, 19, 435–441.

28 Crys Alis Pro, Oxford Diffraction, UK.

29 O. V. Dolomanov, L. J. Bourhis, R. J. Gildea, J. a. K. Howard, and H. Puschmann, *J. Appl. Cryst.*, 2009, 42, 339–341.

30 G. M. Sheldrick, *Acta Crystallogr. A.*, 2008, 64, 112–122.

31 A. L. Spek, *Acta Crystallogr. D.*, 2009, 65, 148–155.

32 A. L. Spek, *Acta Crystallogr. C.*, 2015, 71, 9–18.

33 S. P. Thompson, J. E. Parker, J. Potter, T. P. Hill, A. Birt, T. M. Cobb, F. Yuan, and C. C. Tang, *Rev. Sci. Instrum.*, 2009, 80, 075107.

34 S. P. Thompson, J. E. Parker, J. Marchal, J. Potter, A. Birt, F. Yuan, R. D. Fearn, A. R. Lennie, S. R. Street, and C. C. Tang, *J. Synchrotron Radiat.*, 2011, 18, 637–648.

35 A. A. Coelho, *TOPAS Academic. Version 4.1, 2007, see http//www.topas-academic.net*.

36 A. A. Coelho, *J. Appl. Cryst.*, 2003, 36, 86–95.

37 G. S. Pawley, *J. Appl. Cryst..*, 1981, 14, 357–361.

38 H. M. Rietveld, *Acta Cryst.*, 1966, 20, 508–513.

39 H. M. Rietveld, *Acta Cryst.*, 1967, 22, 151–152.

40 H. M. Rietveld, *J. Appl. Cryst.*, 1969, 2, 65–71.

41 K. K. Tanabe, Z. Wang, and S. M. Cohen, *J. Am. Chem. Soc.*, 2008, 130, 8508–8517.

42 T. Kawamichi, T. Kodama, M. Kawano, and M. Fujita, *Angew. Chemie Int. Ed.*, 2008, 47, 8030–8032.

43 C. Serre, F. Millange, C. Thouvenot, M. Noguès, G. Marsolier, D. Louër, and G. Férey, *J. Am. Chem. Soc.*, 2002, 124, 13519–13526.

44 C. R. Murdock, B. C. Hughes, Z. Lu, and D. M. Jenkins, *Coord. Chem. Rev.*, 2014, 258-259, 119–136.

45 C. Mellot-Draznieks, C. Serre, S. Surblé, N. Audebrand, and G. Férey, *J. Am. Chem. Soc.*, 2005, 127, 16273–16278.

46 C. Serre, C. Mellot-Draznieks, S. Surble, N. Audebrand, Y. Filinchuk, and G. Ferey, *Science.*, 2007, 315, 1828–1831.

47 T. Devic, F. Salles, S. Bourrelly, B. Moulin, G. Maurin, P. Horcajada, C. Serre, A. Vimont, J.-C. Lavalley, H. Leclerc, G. Clet, M. Daturi, P. L. Llewellyn, Y. Filinchuk, and G. Férey, *J. Mater. Chem.*, 2012, 22, 10266-10273.

48 T. Devic, P. Horcajada, C. Serre, F. Salles, G. Maurin, B. Moulin, D. Heurtaux, G. Clet, A. Vimont, J.-M. Grenèche, B. Le Ouay, F. Moreau, E. Magnier, Y. Filinchuk, J. Marrot, J.-C. Lavalley, M. Daturi, and G. Férey, *J. Am. Chem. Soc.*, 2010, 132, 1127–1136.

49 S. A. Moggach, T. D. Bennett, and A. K. Cheetham, *Angew. Chem. Int. Ed.*, 2009, 48, 7087–7089.

50 D. Fairen-Jimenez, S. A Moggach, M. T. Wharmby, P. A Wright, S. Parsons, and T. Düren, *J. Am. Chem. Soc.*, 2011, 133, 8900–8902.

51 F. Millange, N. Guillou, M. E. Medina, G. Férey, A. Carlin-Sinclair, K. M. Golden, and R. I. Walton, *Chem. Mater.*, 2010, 22, 4237–4245.

52 Y. Xiao, T. Han, G. Xiao, Y. Ying, H. Huang, Q. Yang, D. Liu, and C. Zhong, *Langmuir*, 2014, 30, 12229–12235.

53 S. Mukherjee, B. Joarder, A. V. Desai, B. Manna, R. Krishna, and S. K. Ghosh, *Inorg. Chem.*, 2015, 54, 4403-4408.

54 C. F. Macrae, P. R. Edgington, P. McCabe, E. Pidcock, G. P. Shields, R. Taylor, M. Towler, and J. van de Streek, *J. Appl. Cryst.*, 2006, 39, 453–457.

55 P. D. C. Dietzel, R. E. Johnsen, H. Fjellvåg, S. Bordiga, E. Groppo, S. Chavan, and R. Blom, *Chem. Commun.*, 2008, 2, 5125–5127.

56 H. Wu, J. M. Simmons, G. Srinivas, W. Zhou, and T. Yildirim, *J. Phys. Chem. Lett.*, 2010, 1, 1946–1951.

57 W. L. Queen, C. M. Brown, D. K. Britt, P. Zajdel, M. R. Hudson, and O. M. Yaghi, *J. Phys. Chem. C*, 2011, 115, 24915–24919.

58 A. C. McKinlay, B. Xiao, D. S. Wragg, P. S. Wheatley, I. L. Megson, and R. E. Morris, *J. Am. Chem. Soc.*, 2008, 130, 10440–10444.

59 P. K. Allan, P. S. Wheatley, D. Aldous, M. I. Mohideen, C. Tang, J. a Hriljac, I. L. Megson, K. W. Chapman, G. De Weireld, S. Vaesen, and R. E. Morris, *Dalton Trans.*, 2012, 41, 4060–4066.

60 V. K. Peterson, Y. Liu, C. M. Brown, and C. J. Kepert, *J. Am. Chem. Soc.*, 2006, 128, 15578–15579.

61 V. K. Peterson, C. M. Brown, Y. Liu, and C. J. Kepert, *J. Phys. Chem. C*, 2011, 115, 8851–8857.

62 H. Wu, J. M. Simmons, Y. Liu, C. M. Brown, X.-S. Wang, S. Ma, V. K. Peterson, P. D. Southon, C. J. Kepert, H.-C. Zhou, T. Yildirim, and W. Zhou, *Chem. Eur. J*, 2010, 16, 5205–5214.

63 J. Getzschmann, I. Senkovska, D. Wallacher, M. Tovar, D. Fairen-Jimenez, T. Düren, J. M. van Baten, R. Krishna, and S. Kaskel, *Microporous Mesoporous Mater.*, 2010, 136, 50–58.

64 M. Dincă, A. Dailly, Y. Liu, C. M. Brown, D. a Neumann, and J. R. Long, *J. Am. Chem. Soc.*, 2006, 128, 16876–16883.

65 M. Dincă, W. S. Han, Y. Liu, A. Dailly, C. M. Brown, and J. R. Long, *Angew. Chem. Int. Ed.*, 2007, 46, 1419–1422.